2018

Adhesion and mechanics of 2D heterostructures

BOSTON UNIVERSITY

COLLEGE OF ENGINEERING

Thesis

ADHESION AND MECHANICS OF 2D HETEROSTRUCTURES

by

METEHAN CALIS

B.S., Yildiz Technical University, 2014

Submitted in partial fulfillment of the

requirements for the degree of

Master of Science

2018

Approved by

First Reader ______________________________

Joseph Scott Bunch, Ph.D.
Associate Professor of Mechanical Engineering
Associate Professor of Materials Science and Engineering
Associate Professor of Physics

Second Reader ______________________________

Harold S. Park, Ph.D.
Professor of Mechanical Engineering
Professor of Materials Science and Engineering

Third Reader ______________________________

Xi Ling, Ph.D.
Assistant Professor of Chemistry
Assistant Professor of Materials Science and Engineering

DEDICATION

This thesis is dedicated to my wife and family.

ACKNOWLEDGEMENTS

Studying at Boston University is the one of the greatest things that happened to me. During my study, I found opportunities to learn and touch so many new ideas along with discovering myself which I never thought they could exist inside of me. These are invaluable assets which I will carry all along my life. There are lots of people who contributed to this journey which became wonderful lifetime experience for me. I am so grateful that I came across with these amazing people.

First, I would like to thank my advisor, Scott Bunch, for pulling me in very exciting area of scientific researches. His enthusiasm to science and confidence to me are the key factors for completing the thesis. His guidance and kindness helped me to find the correct answers when I encountered failures. All of these were the great inspiration for me to keep continuing what we started.

Next, I would like to thank David Lloyd. I learned much from him. He always answered my big chunks of questions with huge patience. During my experimental studies, his evaluations on my data is crucial part of this thesis. He also taught me everything about two-dimensional material growths, transfer methods and AFM measurements.

Another person I want to thank is Anubhav Wadehra. Together we shared many wonderful memories in lab and in Boston. For my first year, he also became my best friend as well as my trainer in the lab. I will always cherish his friendship.

For the work in this thesis, I would like to thank Santiago J. Cartamil-Bueno for fabricating the first devices on the graphite and Bingjie Hao for performing the first experiment on the MoS_2-Graphite devices. With their contribution, I was able to finish the Chapter 4. I also would like to thank the entire Bunch lab, Lauren Cantley, Kailu Song, Feri Samie Yousefi. They helped me to become familiar with the experimental setups. They were always there for me when I was struggling with the experiment. Furthermore, I want to thank Daniel Gendin, who is my unofficial personal trainer. His great personality and immense knowledge on mechanics, and math broaden my view so much.

I would like to thank Ministry of National Education Turkey and New York Attaché for financially supporting me throughout my graduate study. Without their invaluable contributions, my dreams never came true.

I would like to thank Xi Ling, Harold Park for serving on my defense committee. In addition to being a committee member in defense, the concepts and knowledge I learned from their courses are useful and precious resources for me to enhance my theoretical view. Besides, I want to thank Gerald J. Fine for his mentorship and understanding that helped me to pave my way at academic life.

I want to thank my family. Their support through the years which brought me to Boston University. They never made me feel alone especially during the challenging times.

Lastly, I want to thank my wife, Ayse Calis. She is the greatest person I have ever met. I am blessed to have met her and being accepted me into her life. She is always very supportive, wherever and whenever I need. Best thing in the life is

to know when I have hard times, she will always be there for me to hold my hand. You make our life much easier and more joyful.

Inevitably, I might leave someone deserving my appreciation in helping me complete this thesis. Therefore, I am grateful to all of those who have touched my life to finish my study successfully.

ADHESION AND MECHANICS OF 2D HETEROSTRUCTURES

METEHAN CALIS

ABSTRACT

The thesis examines the adhesive interaction between graphite layers and atomically thin MoS_2 crystals. Vertical van der Waals(vdW) heterostructures are fabricated by stacking different two-dimensional (2D) materials on top of each other. Blister test is used to measure the adhesive interactions between 2D heterostructures and their transferred substrates and between the layers themselves. This adhesive interaction is important in maintaining the mechanical integrity of the device during mechanical loadings and its understanding will help pave the way to the design and fabrication of micromechanical device from 2D heterostructures. Furthermore, applying controlled strains can be used to alter the electrical and optical properties thereby improving efficiency and performance.

At first, we grew MoS_2 and graphene by CVD and stacked the layers on top of each other using a dry transfer method. The MoS_2/graphene heterostructure was then transferred onto pre-etched cavities on a silicon wafer. The blister test was used for controllably introducing strain into the heterostructure. Atomic Force Microscopy was used for measuring the shape of the deformed blister and Raman and Photoluminescence(PL) measured the optical response. The strain mismatch between the biaxial strain and a PL-converted strain suggests crumpling of the graphene layer and a substantial softening of the mechanical response. Lastly, we created graphite holes with photolithography to measure the work of separation

between an atomically smooth graphite surface and MoS_2. We found this value to be at least 320mJ/m^2 which is higher than the MoS_2/SiO_x areas that was previously studied.

TABLE OF CONTENTS

LIST OF TABLES

LIST OF FIGURES

CHAPTER 1. INTRODUCTION

1.1 Introduction

Membranes are important elements that are used in a wide variety of fields such as physical, and biological systems. For example, they could be used in mechanical pressure sensing. Stretched surface of a balloon is great example to explain this phenomenon. We observe the surface tension on membrane because the pressure difference needs to be balanced.

With the discovery of the new materials, researchers have been looking for the ways to identifies their mechanical and electrical properties to use these new material properties for examining the existing problems as well as finding ways to improve the accuracy of the pre-existing problems.

Obtaining the graphene out of graphite was the revolutionary step and led to start high volume of scientific and technological researches on the two-dimensional (2D) materials field[1]. Discovery of the graphene also led to open gates to other 2D materials such as transition metal-dichalcogenides (TMDs, e.g., MoS_2), hexagonal boron-nitride (h-BN), and black phosphorous.

Graphene is not the only material that has been using as a 2D electronic material. Other than the graphene, there are other 2D materials which are used in wide variety of applications in the range from the insulators to metals as well as superconductors.

For 2D materials, atomic bonding between atoms and molecules is much stronger than the forces which hold these sheets out of plane direction. We can obtain these single sheets by layering van der Waals solids. The 2D materials show different phonon and electronic structural properties from their bulk phase. Their unique properties stem from the ability of the quantum confinement of electrons[3] and the absence of interlayer interactions[3].

Graphene is the one of the important example of exhibiting the vdW forces which are used to define the structure and function of 2D materials[4]. Furthermore, adhesive forces have a critical role if we want to model the mechanical behavior of atomically thin materials. With the help of these two forces, we could clamp the material onto the surface which affect materials ability of folding[5], sliding[6], and peeling[7]. An understanding of interplay coupling between the materials, such as the adhesion energy, is also critical during the fabrication of nano-electromechanical systems[8], flexible electronic devices[5], graphene separation membranes[7], and stacked heterostructures formed out of 2D materials.

Blister test and the laminated beam fracture experiments are widely used processes to determine the adhesion between the 2D materials. In some cases, breaking or sliding can be observed during the test which cause to us gather poor quality data from the experiments. To prevent this, another layer is used as supporting layer onto the measured monolayer in order to keep its integrity before delamination starts between the 2D material and substrate. Examples of this approach have been studied by Bunch's group[9] where graphene is suspended over etched microcavities.

1.2 Outline

We carried out the first experiments about work of separation of MoS_2 over the graphite cavities. In addition to these experiment, MoS_2/graphene heterostructural combination is examined to reveal the mechanical behavior of this bilayer configuration. Chapters 1-2 consist of the basic concepts and theoretical aspect which are employed for the experimental results. The experimental section begins in Chapter 3 in which we fabricate MoS_2/graphene heterostructure and transfer those layers onto pre-etched SiO_x microcavities. After introducing pressure, we measure photoluminescence and the mechanical response of these suspended layers. Chapter 4 contains experimental results of the work of separation between atomically thin MoS_2 and graphite holes as well as the result of CVD-growth single layer of MoS_2 mechanical properties. We find that the work of separation of MoS_2/graphite combination is higher than where MoS_2 is located on the SiO_x. The calculated separation energy is also in a range of separation energy of the few layer graphene on the SiO_x (0.31 ± 0.03 Jm^{-2})[9] which leads us to gain insight of the interaction between 2D materials.

1.3 Graphene and Graphite

Graphene is a single atomic layer of sp^2 -bonded carbon atoms arranged in a close-packed honeycomb lattice. Many of graphene's unique properties can be derived from its chemical structure[10,11].

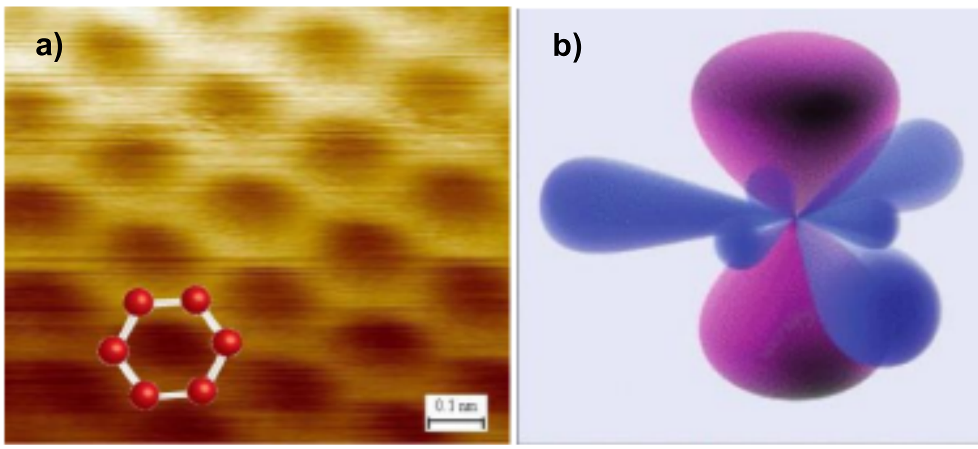

Figure 1.1. a) STM image for graphene b) Chemical structure for carbon atom in graphene[10,11]. (Figure taken from; Elena Stolyarova et al., 2007)

Graphene is the thinnest material in the world, its Young's Modulus is around 1.0 TPa[7] which gives it a robust mechanical characteristic. Graphene is the ultimate limit for membrane applications and chemically stable[12]. It can be wrapped up into 0D buckyballs, rolled into 1D nanotubes or stacked into 3D graphite[13]. The weak van der Waals force is the main bond which helps to hold the graphite layers; on the other hand, there is a strong covalent bonding in-plane direction. Due to the mismatch between in lattice stacks, graphite has the property of super lubricity where the frictional force is reduced considerably[14]. This gives pencils the writing ability as well.

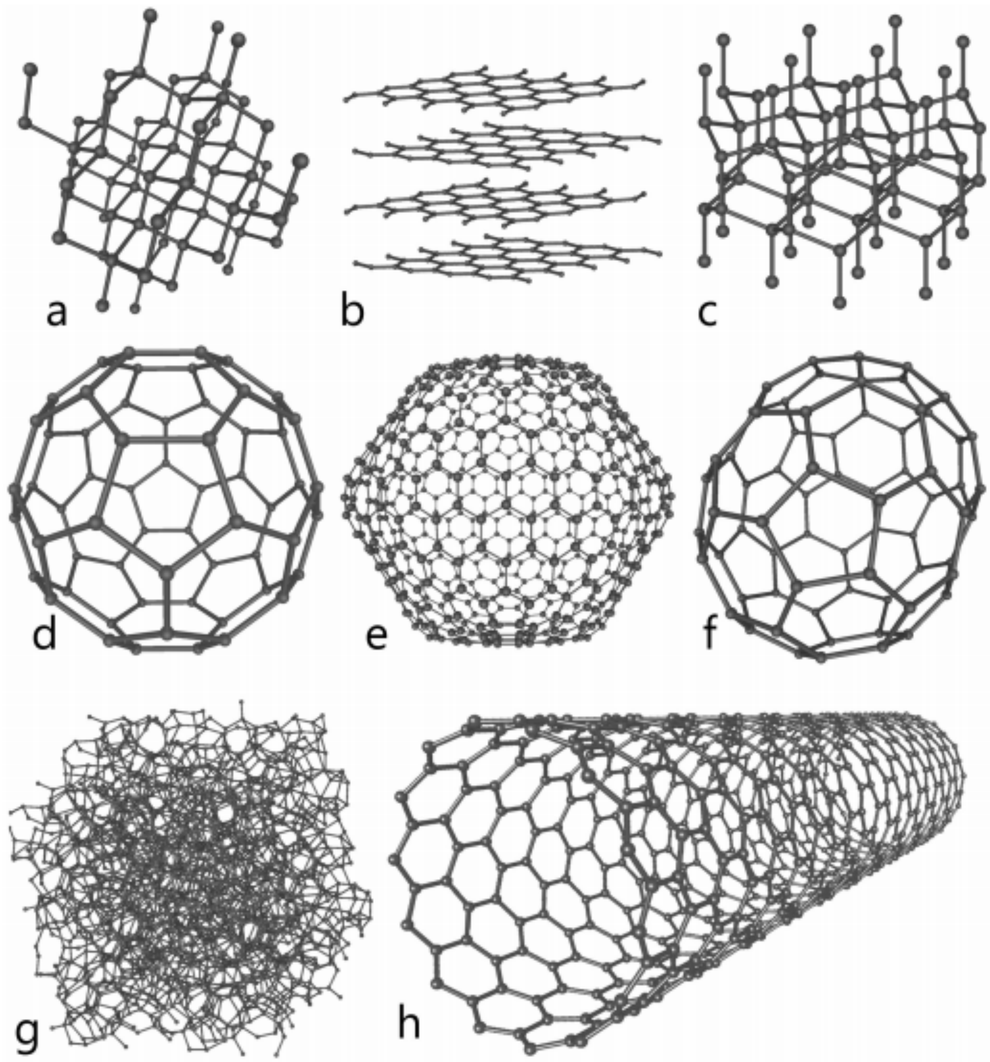

Figure 1.2. Carbon allotropes. a) Diamond, b) Graphite, c) Lonsdaleite, d-f) fullerenes (C60, C540, C70) g) Amorphous carbon, and h) Carbon nanotube. (Figure taken from; Wikipedia.com: Allotropes of Carbon.)

Free-standing graphene has high bending rigidity, $\kappa \simeq 1\ eV$[16]. Other remarkable mechanical properties of the graphene are breaking stress (σ_{int})= *42 N/m* and a breaking strain(ε_{int})= *25%* [20].

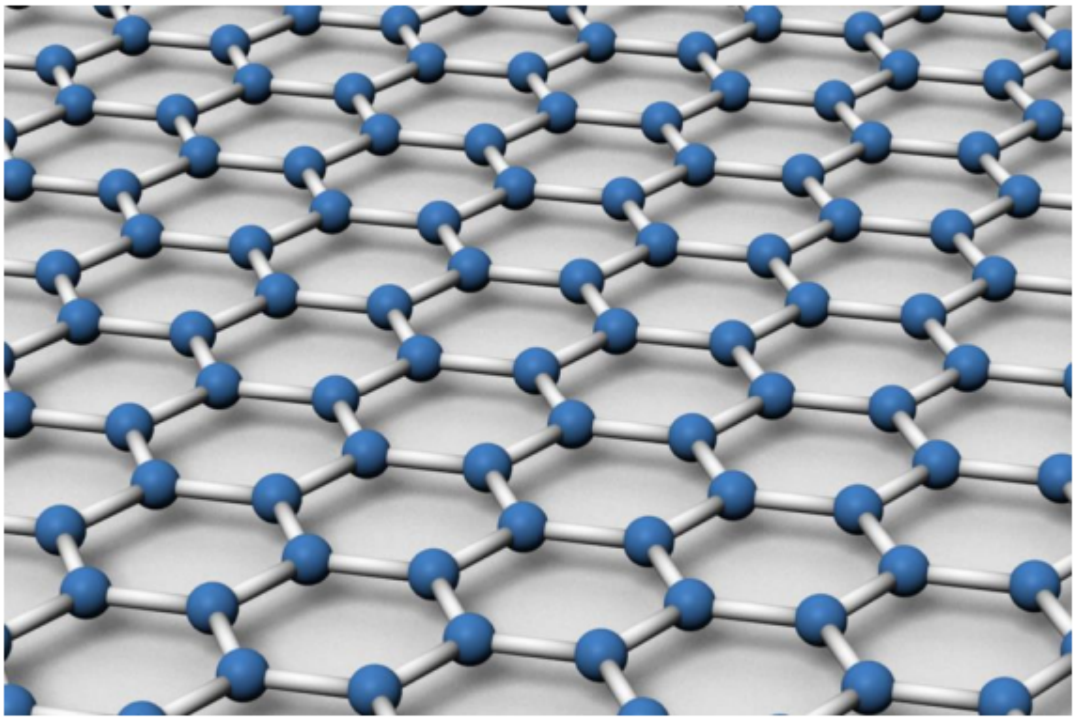

Figure 1.3. Structure of graphene lattice. Carbon atoms are in blue[97]. (Figure taken from; Hedberg, et al.).

It was also proved that graphene is impermeable to all standard gases at room temperature[22]. From the theoretical studies, the impermeability of the graphene can be explained by graphene's high crystal quality, low defect density. The other factor that also helps graphene to show impermeability is that the electron density of graphene's aromatic rings is large enough that atoms and molecules can't pass through [21].

Table 1.1. Properties of pristine graphene (Table taken from; Koenig, S. thesis)

Property	**Symbol**	**Value**
C-C bond length	d	1.42 Å
Graphite interlayer spacing	w	3.35 Å
Optical Absorbance (per layer)	A	2.3%
Young's Modulus	E	1 TPa
Poisson ratio	v	0.16
Breaking Stress	σ_{max}	42±4 N/m
Breaking Strain	ε_{max}	0.25
Intrinsic bending rigidity (monolayer)	B	1-2 eV

The initial researches were focused on graphene, because of its unusual electronic features. The most outstanding electronic feature of graphene is its unique band structure because of its two-dimensional nature. Graphene has a peculiar band structure which brings with a zero bandgap semiconductor that touches at the corners of the first Brillouin zone[15].

Graphene has been used in variety of applications since its electronic properties. graphene absorbs *2.3%* of light *so* it is nearly transparent, it could be used in touch screen and current collectors in solar cells [19].

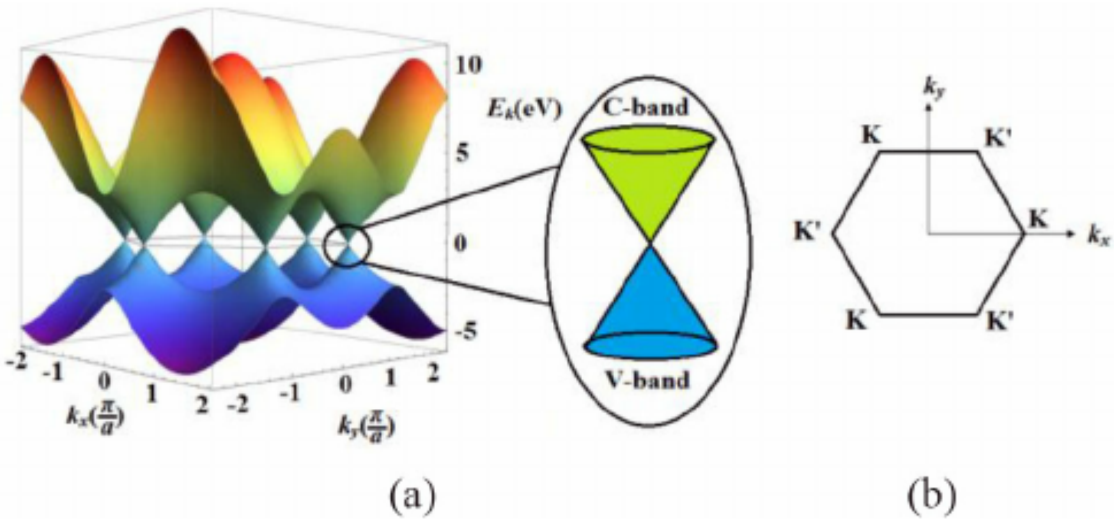

Figure 1.4. Dispersion relation of graphene. a) Dirac point of the graphene where the six cones of the conduction and the valance bands are touching. There is no bandgap in between[17]. b) Because of the symmetry, six Dirac points can be reduced to two equivalent points K and K'[18].
(Figure taken from; The Nobel Prize in Physics 2010 — Advanced Information, http://www.nobelprize.org/nobel_prizes/physics/laureates/2010/advanced.html)

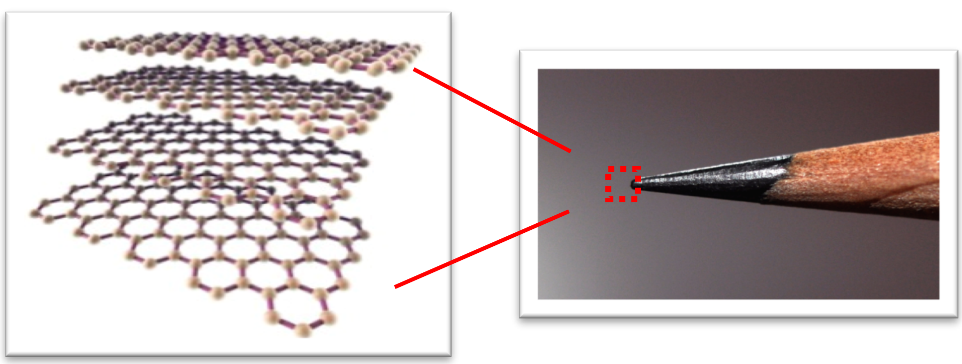

Figure 1.5. Graphite layers (Figure taken from: Charlotte McLeod et al., Saint Jean Carbon Inc., 2016)

1.3.1 Graphene Fabrication

There are four primary ways to make graphene. First, the easiest and traditional way is mechanical exfoliation. Technique for obtaining single layer of graphene out of graphite is also known as the 'Scotch Tape Method'[23]. This method has been around for centuries which is also known by writing with a pencil. By writing, we create many graphene sheets spread over paper. The disadvantage of this method is that we can't control the thickness of the sheets which they vary so much. The Scotch tape method was born upon this idea. For this method, we place a piece of graphite on Scotch tape, then stick the tape together and peel it apart until the tape is covered with a thin layer of graphite. Then one is able to produce graphene on the targeted substrate[4]. Furthermore, If the correct oxidized thickness is used for substrate during process, we will be able to distinguish the layer thickness of the graphene flakes under the optical microscope[24]. With Scotch tape technique, we can have benefit of producing high quality of graphene. One of the main drawbacks of this technique is we can only produce for small scale. For the case of finding suspended graphene device could take several days or weeks.

Dispersing the graphene from the solution is another common graphene fabrication technique. Similar to the exfoliation process, in the intercalating, process consists of introducing foreign molecules in between in order to separate the graphene layers of graphite. This method is remarkable with respect to the fact that it uses Bronsted acids to separate the layers[25]. However, the process is very delicate and has to improve on its stability before we will see it being widely used.

Another method is that graphene can be created from epitaxial growth[26,27]. After heating up SiC in argon, Si will sublimate. The residue carbon atoms will assemble into graphene layers. But one drawback of SiC is the expensive price of the material.

The most common used growth method is chemical vapor deposition (CVD) which we use in experiments. There are two widely used catalysts, nickel[28] and copper[29]. The graphene growth on copper is a surface-catalyzed process, wherein surface decomposition of the precursor leaves carbon atoms that assemble into the 2D graphene without carbon intercalation into the metal[29]. Quality of CVD graphene mainly focused on process details like changing C:H ratio[30], tuning the H_2 and hydrocarbon (CH_4) gas pressures[31], and smoothing the surface of copper foil[32]. Carbon nanotubes and diamond are successfully fabricated with CVD method.

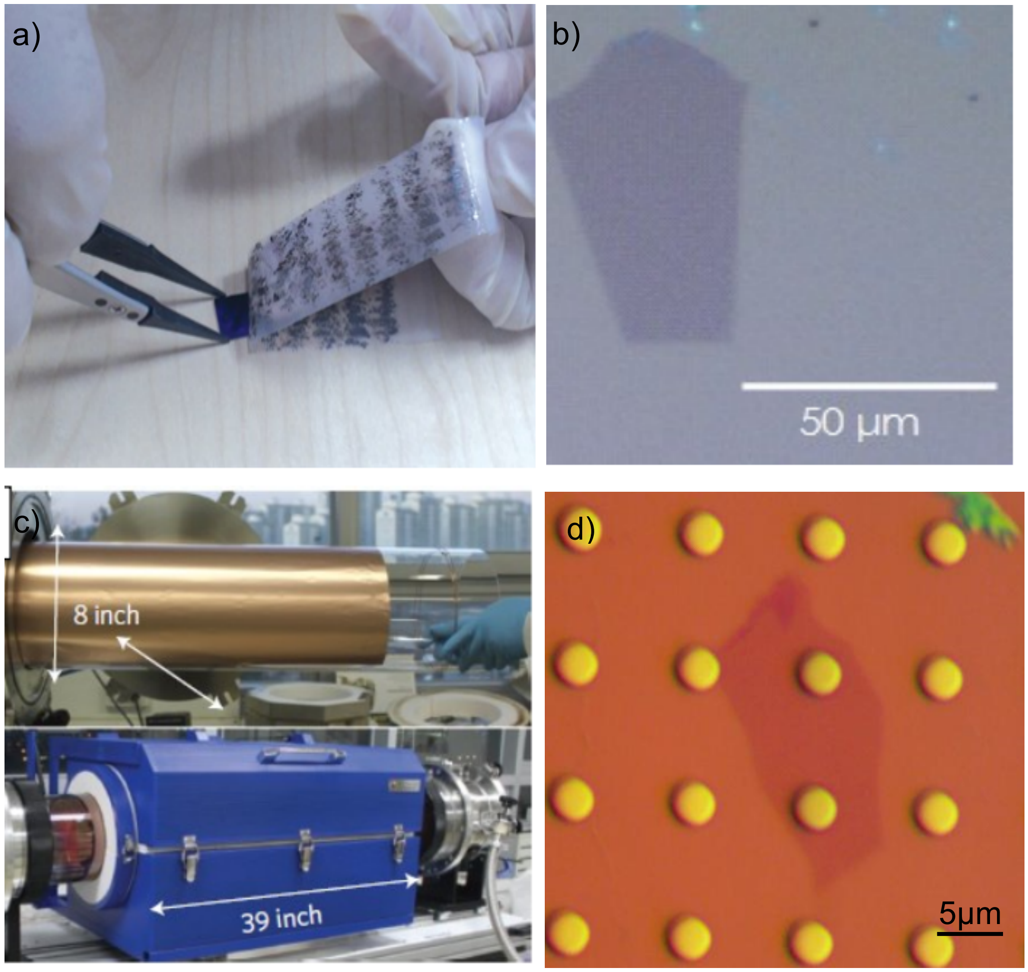

Figure 1.6. a) Scotch tape method[33] (Figure taken from; Noorden et al., 2012) b) Optical image of exfoliated graphene flake.[35] (Figure taken from; Koeing et al., 2013) c) CVD growth method preparation in furnace[34]. d) Optical image of graphene flake exfoliated onto pre-etched micro cavities.

1.4 Transition Metal Dichalcogenides (TMDC)

Transition metal dichalcogenides has the the formula of MX_2 (where M is a transition metal and X is a chalcogen). TMDCs can be used in various applications due to its electronic properties in the range from insulator to semiconductor. Each TMDC could show variety of electronic characteristics which stem from nonbonding d-bands that comes from the transition metal electrons[36]. Therefore, with advent of these 2D materials, we would obtain the unprecedented electronic features which we never obtained from the conventional materials those were previously used.

Table 1.2. Different TMDCs Growth Using Various Techniques[37] (Table taken from; Bhimanapati et al., 2015)

Technique		Mono- and few-layer materials available to date					Achievements	Challenges
		Single phase TMD	*TMD alloy*	*Doped TMD*	*Vertical heterostructures*	*Lateral heterostructures*		
Top-down	Mechanical exfoliation (and CVT)	1T, 2H MoX_2 1T, 2H WX_2 BP,SnX_2, 1T, 2H $(Nb,Ti,Zr,Nb,Ta)X_2$	$Mo_xW_{1-x}S_2$ $Mo_xW_{1-x}Se_2$	Au-doped MoS_2, Re-doped MoS_2, Nb-doped MoS_2	2H (MoS_2-WS_2), 2H (MoS_2-WSe_2), 2H MoS_2-graphene, 2H WS_2-graphene, 2H MoX_2-hBN,2H WX_2-hBN, 2H WSe_2-1T $SnSe_2$, 2H MoS_2-BP	-	High crystallinity	Thickness control, yield, not scalable
Top-down	Liquid exfoliation	1T,2H MoX_2 1T,2H WX_2,2H TiS_2,2H TaS_2, $(Nb,Ti,Zr,Nb,Ta)X_2$	-	-	-	-	High scalability	Small crystallites, thickness control, yield.
Bottom- up	Powder Vaporization	1T, 2H MoX_2 1T, 2H WX_2	MoS_xSe_{2-x} $Mo_xW_{1-x}S_2$	Mn-doped MoS_2 Co-doped MoS_2	1T MoX_2-2H MoX_2, 2H MoX_2-2H WX_2,2H MoS_2-BP, 2H MoX_2-GR, 2H WX_2-GR, 2H MoS_2-2H WSe_2-GR, 2H WS_2-hBN, 2H MoS_2-SnS_2, 2H WS_2-SnS_2, 2H WSe_2-SnS_2	Graphene-hBN, 1T MoS_2-2H MoS_2, 2H MoS_2-WS_2 2H MoX_2-2H MoX_2 2H WX_2-2H WX_2	High scalability	Defect control, uniformity, stoichiometry control
Bottom- up	MOCVD	1T MoX_2, WX_2	-	-	MoS_2-WSe_2-graphene	-	High scalability	Defect control
Bottom- up	MBE	2H $MoSe_2$ 2H WSe_2 1T $PtSe_2$	-	-	$MoSe_2$-graphene	-	High scalability	Defect control, domain size

X- S,Se, BP- Black phosphorous, GR- graphene

TMDCs have drawn so many researchers' attention, because we can obtain high quality, atomically-thin layers by utilizing exfoliation method[38]. On the other hand, TMDS gives us control over the electrostatic field-affect which arises from the lack of surface dangling bonds[38]. Hence, TMDCs have been becoming more popular research area, also we can understand that from looking publication numbers which are devoted to class of TMDC in Figure 1.7.

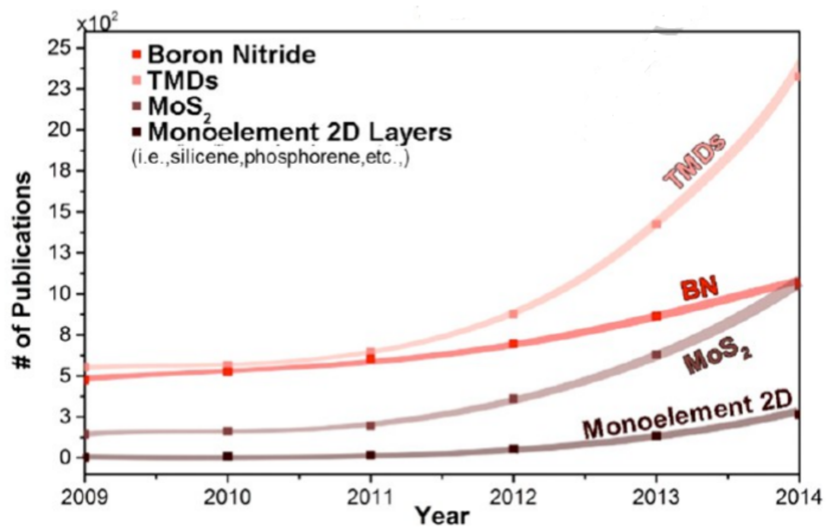

Figure 1.7. Publication trends in 2D materials. (Image taken from; Web of Science)

1.5 MoS_2

The transition-metal dichalcogenide semiconductor MoS_2 has attracted great interest because of its prominent electronic, optical properties.

MoS_2 has an indirect gap at 1.2 eV for its bulk phase and a direct gap at 1.8 eV for its monolayer phase[39]. The band structure of MoS_2 can also shift in response to strain in the material. Experiments have shown that the optical band gap reduces by ~50 meV/% for uniaxial strain [40] and ~100 meV/% for biaxial strain[41].

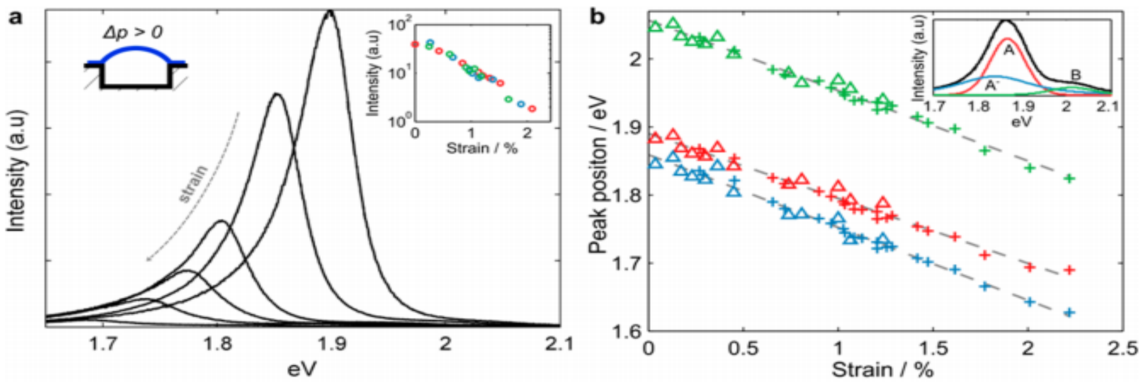

Figure 1.8. a) PL measurement for a monolayer MoS_2 with corresponding to different strain[41]. b) Shifting in peak positions of the A, A', and B peaks due to change in strain. (Image taken from; Lloyd et al., 2016)

The direct band gap in monolayer MoS_2 also makes it a promising material for optoelectronic applications. We can't observe the photoluminescence in the bulk structure of MoS_2 due to its excitonic absorption.

MoS_2 is also shown to have good mechanical strength. Its in-plane stiffness is *~180 N/m*, corresponding to an effective Young's modulus of *270 GPa*. Breaking occurs at when the breaking strength is *~15 N/m* with an effective strain between *6 – 11%* when measured via nano-indentation experiments[43]. MoS_2 is appropriate to use in flexible electronics/optoelectronics applications.

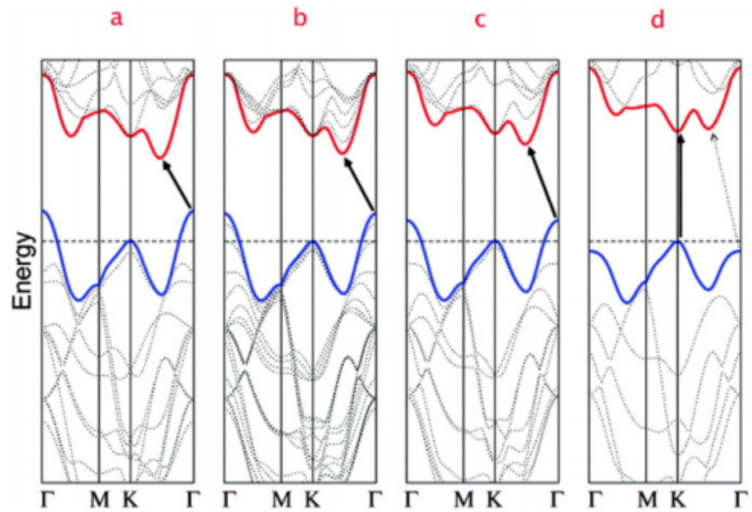

Figure 1.9. Band structure of MoS_2 calculated by density functional theory for a) Bulk, b) Quadlayer, c) Bilayer, and d) Monolayer [42] (Figure taken from; A. Splendiani, L. Sun et al., 2010)

1.5.1 MoS2 Fabrication

The fabrication of 2D MoS_2 is similar to graphene in several aspects: two main preparation methods are mechanical exfoliation and CVD method. Exfoliation method shows parallelism with graphene Scotch tape method. If we want to fabricate the single or multiple layer(s) MoS_2 from its bulk single crystal, we can simply use the Scotch tape method again to produce high quality flakes. The percentage of successfully obtaining monolayer is also low as it is observed in graphene case and it is limited to small scale. On the other hand, the monolayer MoS_2 single crystal grown with CVD reaches length scales of up to 100 μm. We used CVD-growth MoS_2 in all experiments.

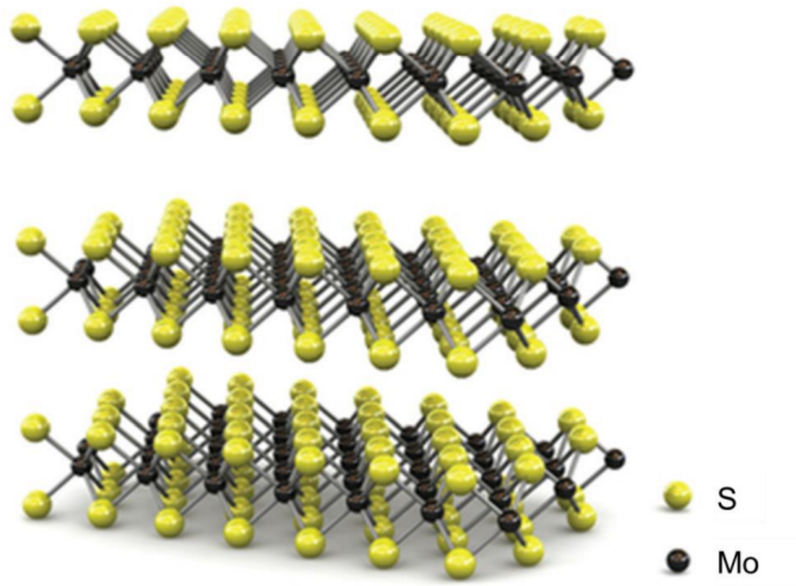

Figure 1.10. Atomic structure of molybdenum disulfide[105] (Figure taken from; B. Radisavljevic et al., 2011)

1.6 2D Materials and van der Waals Heterostructures

2D materials have much stronger in-plane atomic bonding than the out-of-plane direction. Using 2D materials in the applications provide us advantage on the tuning their electronic properties. The band-gap engineering turns out to be remarkable approach that can be implemented by changing the number of layers in a given material[45]. Moreover, 2D materials possess remarkable properties such as being exceptionally strong, lightweight, and excellent conductors of heat.

Table 1.3. 2D materials family[13] (Table taken from; A. K. Geim et al., 2013)

Graphene family	Graphene	hBN 'white graphene'	BCN	Fluorographene	Graphene oxide
2D chalcogenides	MoS_2, WS_2, $MoSe_2$, WSe_2	Semiconducting dichalcogenides: $MoTe_2$, WTe_2, ZrS_2, $ZrSe_2$ and so on	Metallic dichalcogenides: $NbSe_2$, NbS_2, TaS_2, TiS_2, $NiSe_2$ and so on	Layered semiconductors: GaSe, GaTe, InSe, Bi_2Se_3 and so on	
2D oxides	Micas, BSCCO	MoO_3, WO_3	Perovskite-type: $LaNb_2O_7$, $(Ca,Sr)_2Nb_3O_{10}$, $Bi_4Ti_3O_{12}$, $Ca_2Ta_2TiO_{10}$ and so on	Hydroxides: $Ni(OH)_2$, $Eu(OH)_2$ and so on	
	Layered Cu oxides	TiO_2, MnO_2, V_2O_5, TaO_3, RuO_2 and so on		Others	

2D materials come along with unique electronic properties which make them great candidates for electronic applications. They could be exploited in wide variety of scopes from superconductors, metallic materials, semimetals, semiconductors to insulators [46].

Recently, researchers have been focusing on 2D heterostructures which are made by combining different 2D materials by using different methods for fabrication. The basic principle is that taking a monolayer and putting it on top of another monolayer or few-layer crystal. Strong covalent bonds maintain the in-plane stability of 2D crystals. On the other hand, even the van der Waals force is not as strong as the covalent bonds, it is sufficient to keep the stack together. Interest upon 2D heterostructures have been growing day by day because we can use the different properties of the different materials on one device which we won't be able to hold such various features with using only one material. If we would like to understand the electronic properties of these heterostructures, we should study the interfacial band alignments and interaction between the 2D materials.

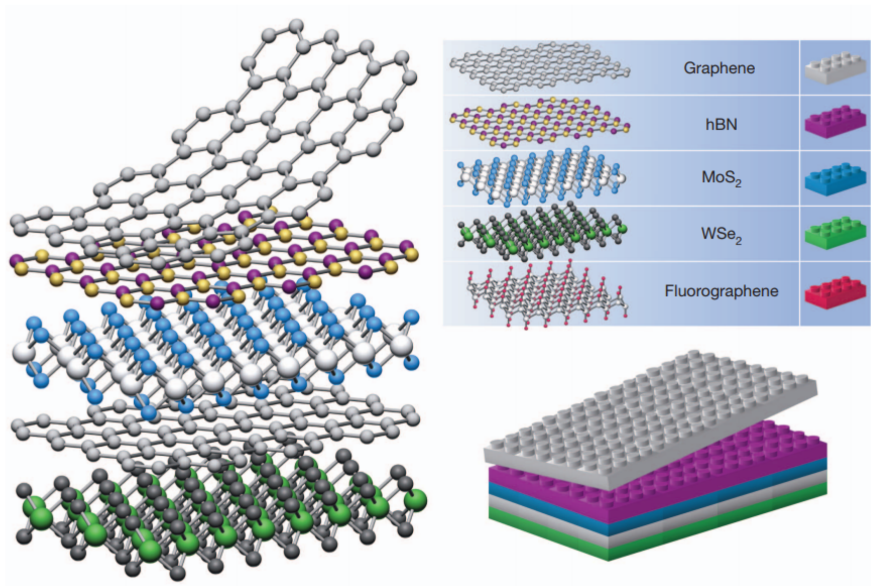

Figure 1.11. Fabrication schematic of the vdW heterostructure[13] (Figure taken from; A. K. Geim et al., 2013)

For example, using atomic layers of h-BN as a substrate, heterostructure of graphene and MoS_2 FETs have been demonstrated with over tenfold mobility enhancement, with remarkable stability even under harsh conditions[48]. Another application is the MoS_2/graphene heterostructure resonators. Exfoliated graphene and CVD-growth MoS_2 is transferred top of each other (Fig1.12.). The heterostructure devices exhibit robust resonances up to ~100 MHz in the VHF band, with a figure-of-merit as high as $f_0 \times Q \approx 8.7 \times 10^9$ Hz[49].

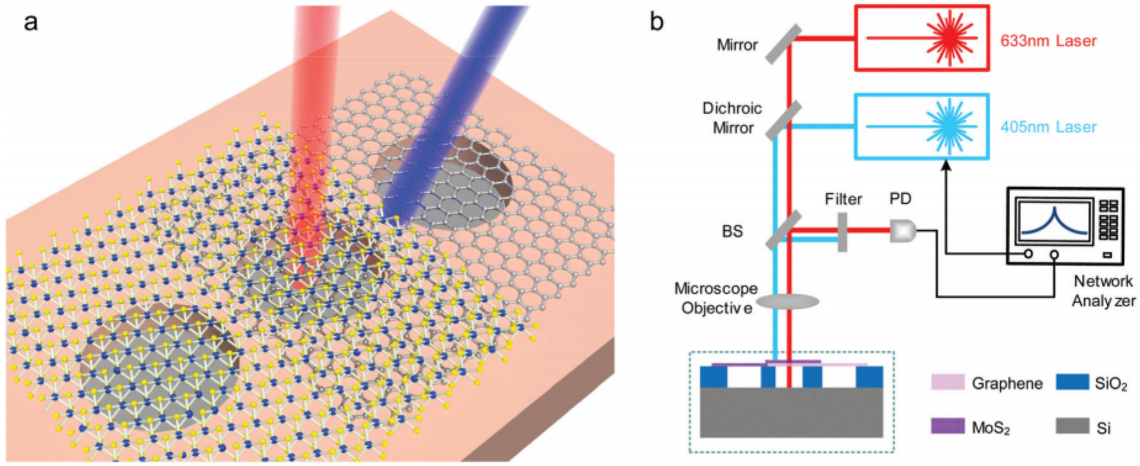

Figure 1.12. a) Schematic of freestanding vdW heterostructure of MoS_2/graphene atomic layers. b) Schematic of the nanomechanical resonance interferometry measurement system[49] (Figure taken from; Fan Ye et al., 2017)

1.7 Raman Spectroscopy

Raman spectroscopy is a fast and nondestructive technique that utilizing vibrational modes to analysis crystal structure. The basic principle of the Raman measurement is that we excite the materials with monochromatic laser that causes the vibration in the lattice. Then we try to detect the inelastic scattering which helps us to calculate the energy shift. Obtained molecular vibrations information is used for sample identification and quantitation. Furthermore, with the information we obtain from the Raman can help us to verify the number of layer [50], probe defects in the crystal lattice[51], determine the amount of strain[52], and measure thermal conductivity[53]. Raman spectroscopy provides high resolution, along with structural and electronic information of the materials[54].

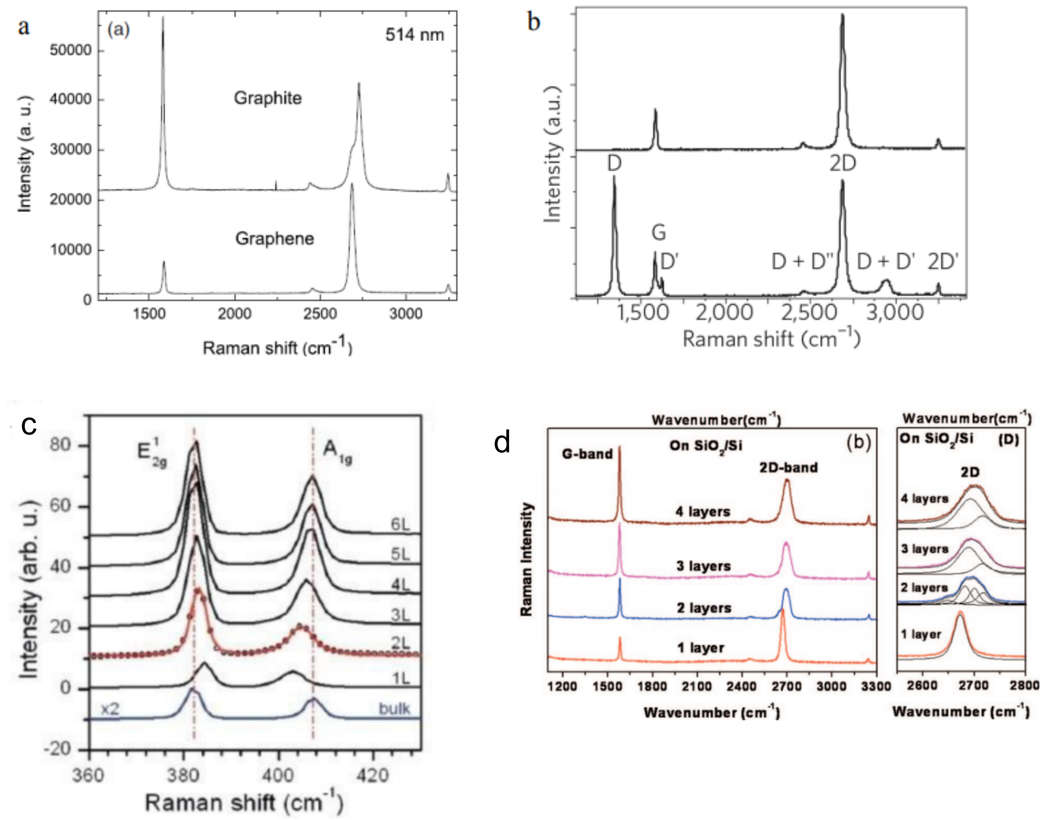

Figure 1.13. a) Raman Spectrum of graphite and exfoliated graphene[50] b) Raman spectrum graphene without defect (top) and with defects (bottom) [51] c) Raman spectrum for different thickness of MoS_2[55] d) Raman spectroscopy of graphene it respect to various layer thickness.[82] (Figures taken from; Yi Zhang et al., 2013)

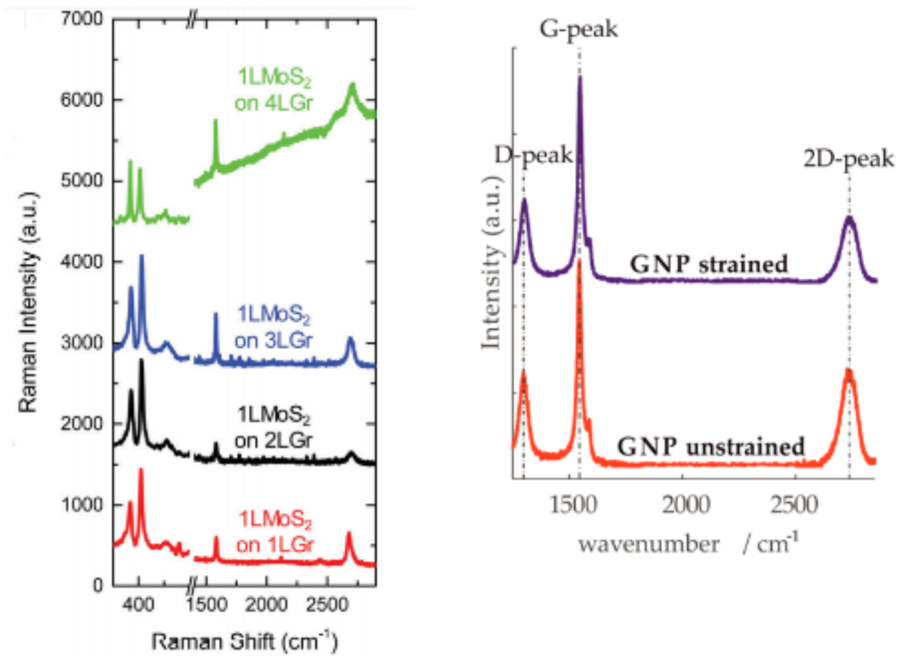

Figure 1.14. a) Graphene and MoS_2 Raman scan with various layer thickness[49] b) GNP Raman scan under unstrained/strained conditions[83] (Figures taken from; V. Yokaribas et al., 2015)

In Figure 1.14., it is shown that the strained graphene shows higher intensities. In Chapter 3, we have measured the Raman spectroscopy of MoS_2 and graphene on the suspended area.

1.8 Atomic Force Microscope (AFM)

The atomic force microscope (AFM) uses a very sharp tip to probe and map sample topography. AFM has two operational modes; *(i) static modes* and *(ii) dynamic modes.* In static modes, the cantilever statically deflects, but the feedback loop tries to maintain its previously determined value of deflection during scanning. In the dynamic modes, the cantilever oscillates at a desired frequency, and for this time the feedback loop tries to maintain previously determined amplitude of oscillation. In static modes, cantilever physically gets contact with the surface during the examination. The most widely used dynamic mode is the *intermittent contact mode*, also called the *tapping mode*. By using the tapping mode, we try to avoid possible damage to sample during scanning. In our measurements we used tapping modes.

1.9 Conclusion

Some fundamental concepts were introduced in this chapter to pave the way for following chapters. In this chapter, it is started with brief introduction of the graphene and graphite, then followed by MoS_2 and other 2D materials as well as heterostructural blocks. In addition to those, we briefly mentioned Raman spectroscopy and AFM which were utilized during the experiment to obtain data. In the next chapter, we will examine the theoretical approaches to define mechanical properties of our devices.

CHAPTER 2. NANOMECHANICS

2.1 Mechanical Properties of Materials

Hooke's law is the fundamental approach to define the mechanical properties of the engineering materials. It can be thought as the analogue of the Ohm's Law. The formula can be written for the material which the force is acting at one direction:

$$\sigma = \frac{F}{A} \tag{2.1}$$

where the σ is stress, F is applied force, and A is area.

If we apply a uniaxial compressive or tensile stress to the material, the relation can be expressed as:

$$\sigma_x = E\,\varepsilon_x \tag{2.2}$$

where ε is strain, and E is the Young's modulus. This claims the material as an isotropic which means that there is no specific crystal orientation.

If we apply shear loading to the material, we can write an equation as:

$$\tau = G\,\gamma \tag{2.3}$$

where τ and γ are the shear stress and strain, respectively. G is named as the shearing modulus of elasticity.

If the material is caused the strain in one direction it would contract in the perpendicular direction to the applied strain. The ratio of the strains in these 2 directions is defined as Poisson's ratio:

$$\upsilon \equiv -\frac{\varepsilon_y}{\varepsilon_x} \quad (2.4)$$

For example, the cork of a wine bottle has $v \sim 0$, rubber has $v \sim 0.5$. Some materials in a class of exotic materials have $v < 0$

In this thesis, we focus on the membranes, which are identified as a special kind of shell incapable of conveying shear loads. In other words, bending can be ignored in membranes[56].

To understand the mechanics in membranes, we can consider a part of a spherical shell of radius *R* and thickness *t*, under a uniform pressure of *P*. The compressive direct stress is:

$$\sigma = -\frac{P\,R}{2\,t} \quad (2.5)$$

The shell bending moment is

$$M = -\frac{P\,t^2}{24} \quad (2.6)$$

So, the bending stress is given by

$$\sigma_b = -\frac{P}{4} \quad (2.7)$$

The ratio between the direct stress to the bending stress

$$\frac{\sigma}{\sigma_b} = \frac{2R}{t} \quad (2.8)$$

From this result, in 2D membranes, *t* is the atomic thickness with a few angstroms and *R* is in micron size, leading to the ratio between 10^3 and 10^4. Hence, as we mentioned before bending stress is negligible in the 2D membranes.

For the biaxial strain, the x and z component of strain are equivalent: $\varepsilon_x = \varepsilon_z = \varepsilon$ which means that pressure difference, as in the spherical balloon example, creates equal strains to both directions.

2.2 Blister Test

Measuring interfacial adhesion between layers is important in terms of scientific and commercial applications[99]. There are several conventional techniques which are used to find out the adhesion energy between the dissimilar interfaces such as the pull-in, double cantilever, and peeling tests[100]. The peeling test is the widely used method to measure adhesion energy of the films. Plastic deformation at fixtures and high bending angles are the main drawbacks of this method[101]. Blister test has been used to overcome all of these disadvantages[102]. The first studies were done by Dannenberg (1961), where, he used pressurized mercury to cause delamination from the surface. On the other hand, Dannenberg preferred a groove shaped crack (rather than circular pattern) to measure the separation energy between the polyurethane elastomer and rigid flat substrate[103]. However, the biggest challenge of this method is when the blister starts to delaminate, the transition happens so quickly that it causes the membrane to collapse before performing the measurements on it. Williams and his co-workers (1969) developed a new approach to the blister test which is used today. This newly developed approach involves increasing the pressure until layer starts to show delamination[104]. Williams employed the Hencky's model of elastically deformed membranes (1915). Further studies were done by Hinkley (1983), and

Briscoe and Panesar (1991) were the pioneer researchers on developing the blister test. Wan and Mai (1995) suggested a change to the blister test that makes it more stable. Instead of increasing the pressure constantly up to critical point, they utilized the isothermal expansion of a fixed number of gas molecules inside the sealed microcavity.

In this thesis, we used the blister test to determine the mechanical properties of our membranes such as the elastic constant. This is also known as the bulge test if we only measure the mechanical properties of the thin films. Furthermore, after delamination occurs, the blister test can be used to determine the adhesion energy between the layer and substrate. In following sections, we will focus on the relevant theoretical approach to the blister test method.

2.3 Membrane Dynamics and Theory

2.3.1 Hencky's Membrane Solution

Von Karman equations give us series of solutions[69]. From these equations, we would end up with relations that are related to maximum deflection, pressure difference across the membrane, and the radius of the membrane. One of the assumption was made by Hencky is uniform lateral loading affects over the membrane. Governing equations for radial and lateral equilibrium are,

$$\sigma_\theta = \frac{d}{dr}(r\,\sigma_r) \tag{2.9}$$

$$\sigma_r \frac{dz}{dr} = -\frac{p\,r}{2\,w} \tag{2.10}$$

where σ_θ and σ_r are the circumferential and radial stresses, respectively, *w* is the thickness, *r* is the radial coordinate, and *p* is the uniform pressure load. The stress-strain relations are[70]

$$\sigma_\theta - v\sigma_r = E\ w\ \varepsilon_\theta \tag{2.11}$$

$$\sigma_r - v\sigma_\theta = E\ w\ \varepsilon_r \tag{2.12}$$

where *E* elasticity modulus, ε_θ and ε_r are circumferential and radial strains, respectively.

The strain-displacement relationships are

$$\varepsilon_\theta = \frac{u}{r} \tag{2.13}$$

$$\varepsilon_r = \frac{du}{dr} + \frac{1}{2}\left(\frac{dw}{dr}\right)^2 \tag{2.14}$$

where the *u* is radial displacement. The boundary conditions at the clamped edges

$$z(a) = 0 \tag{2.15}$$

$$u(a) = 0 \tag{2.16}$$

where *a* is the radius of the circular region of the membrane being pressurized. Combining equations (2.9) through (2.16) the resulting equations are

$$\frac{r}{E\ w}\frac{d}{dr}\left[\frac{d}{dr}(r\sigma_r) + \sigma_r\right] + \frac{1}{2}\left(\frac{dz}{dr}\right)^2 = 0 \tag{2.17}$$

$$\sigma_r\left(\frac{dz}{dr}\right) = -\frac{1}{2}\ p\ r \tag{2.18}$$

Substituting equation (2.18) into equation (2.17) gives

$$\frac{{\sigma_r}^2}{E\ w}\frac{d}{dr}\left[\frac{d}{dr}(r\sigma_r)+\sigma_r\right]+\frac{1}{8}p^2r=0 \quad (2.19)$$

Then, Hencky gave a series solution to this equation as

$$\sigma_r=(\frac{E\ p^2a^2}{64\ w^2})^{\frac{1}{3}}\sum_{n=0}^{\infty}B_{2n}(\frac{r}{a})^{2n} \quad (2.20)$$

with $B_2= -1/B_0^2$, $B_4= -2/3\ B_0^5$, $B_6= -13/18\ B_0^8$, $B_8= -17/18\ B_0^{11}$, $B_{10}= -37/27\ B_0^{14}$, and so on. B_0 is a function of the Poisson ratio, *v*. We would obtain circumferential stress and the deflection profile, respectively

$$\sigma_\theta=(\frac{E\ p^2a^2}{64\ w^2})^{\frac{1}{3}}\sum_{n=0}^{\infty}(2n+1)B_{2n}(\frac{r}{a})^{2n} \quad (2.21)$$

$$z(r)=(\frac{pa^4}{Ew})^{\frac{1}{3}}\sum_{n=0}^{\infty}A_{2n}[1-\left(\frac{r}{a}\right)^{2n+2}] \quad (2.22)$$

with $A_0= 1/B_0$, $A_2= 1/2\ B_0^4$, $A_4= 5/9\ B_0^7$, $A_6= 55/72\ B_0^{10}$, and so on. Furthermore, we can get the expression for the maximum deflection, δ, for the membrane at $r=0$, $\delta=z\ (0)$;

$$\delta=(\frac{pa^4}{Ew})^{\frac{1}{3}}\sum_{n=0}^{\infty}A_{2n} \quad (2.23)$$

We can manipulate (2.23) to get the pressure difference as a function of the Young's modulus, radius and maximum deflection of membrane as by the help of following formulas;

$$K(v)=\sum_{n=0}^{\infty}(1/\ A_{2n})^3 \quad (2.24)$$

$$\Delta p=K(v)(E_{2D}\delta^3)/a^4 \quad (2.25)$$

By integrating *z(r)* over the microcavity area using equation (2.22), we can find the volume under the blister as;

$$V_b = \int z(r)\, 2\,\pi\, r\, dr = C(v)\pi a^2\, \delta \qquad (2.26)$$

The constants *K(v)* can be found by solving for B_0 by satisfying the boundary condition *u(a)=0*,

$$\frac{d}{dr}(r\,\sigma_r) - \nu\sigma_r|_{r=a} = 0 \qquad (2.27)$$

Or

$$(1-v)B_0 + (3-v)B_2 + (5-v)B_4\,(7-v)B_6 + \;... = 0 \qquad (2.28)$$

After that, we can find out the *C(v)* by using equations (2.22), (2.23), (2.26) which lead us to

$$C(v) = 1 - \; 2 * (K(v))^{1/3} * \frac{[\int_0^r r * (\sum_{n=0}^{\infty} A_{2n}\left(\frac{r}{a}\right)^{2n+2})\, dr]}{a^2} \qquad (2.29)$$

2.3.2 Biaxial Strain

We will utilize the equations (2.9) (2.12) (2.20) (2.25) to find biaxial strain. To solve these equations, we should define the boundary conditions first. At *r=0* $\sigma_\theta = \sigma_r$ and $\varepsilon_\theta = \varepsilon_r$. These conditions lead us to

$$\sigma_r(0) - \nu\sigma_\theta(0) = E\; w\; \varepsilon_r(0) \qquad (2.30)$$

$$\varepsilon_r(0) = \; \sigma_r(0)\; \frac{(1-v)}{E\,w} \qquad (2.31)$$

From equation (2.25), if we plug in *r=0*, we would end up with

$$\sigma_r(0) = \frac{1}{4}\frac{(1-v)}{E\,w}\;B_0\,q^{\frac{2}{3}} \tag{2.32}$$

where $q = \frac{\Delta p\,a}{E\,w}$. Finally, if we plug in q and equation (2.25) back to (2.31), we will have

$$\varepsilon_b = (\frac{\delta}{a})^2\,\frac{(1-v)B_0\,K(v)^{2/3}}{4} \tag{2.33}$$

2.3.3 Thermodynamic Model of the Blister Test

We determine the work of separation Γ_{sep} by using the values for P_0, δ and *a*. In our model the behavior of the blister is considered under three stages. First, the system is at equilibrium with the membrane flat and stress free and the pressure inside and outside the cavity equal to P_0. After placing the device into pressure chamber, gas leaks into cavity. The gas inside the cavity is assumed to isothermally expand to it final equilibrium pressure P_{int}.

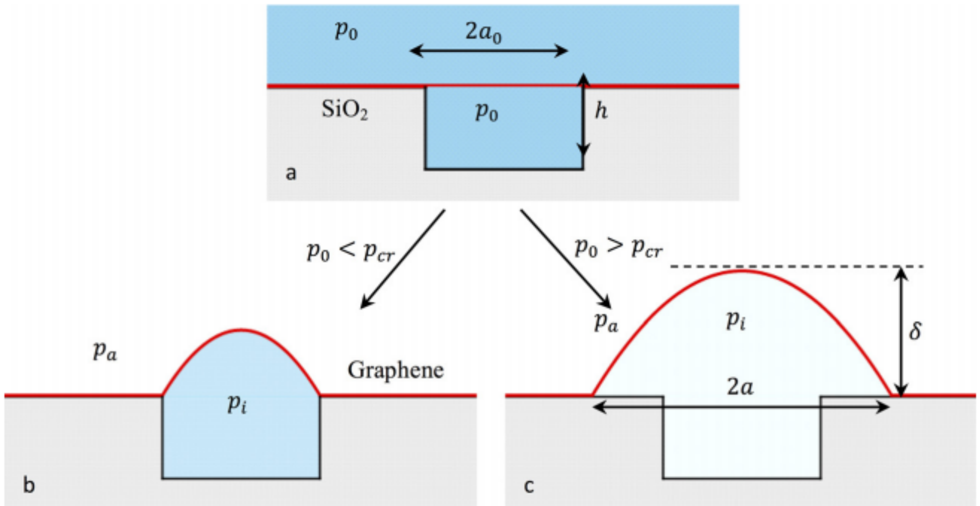

Figure 2.1 Schematic of the microcavity sealed with 2D membrane a) the initial configuration, charged with pressure P_o in the pressure chamber. b) No delamination after taking out of from the pressure chamber c) Delamination occurred from the substrate after taking out of from the pressure chamber.[71] (Figure taken from Boddeti, N. G et al., 2013)

We consider to determine equilibrium configuration of the deformed membrane by seeking minima in the system free energy, *F*. The free energy of the system can be expressed as;

$$F = F_{mem} + F_{gas} + F_{ext} + F_{adh} \tag{2.34}$$

F_{mem} originates from membrane deformation which the deformation on the membrane creates strain energy while balancing the pressure difference. For a fixed *a*, we can compute F_{mem} assuming quasi-static expansion of the gas using equations (2.23) and (2.26)

$$F_{mem} = \int\int N_i \; d\epsilon_i \; dA_{mem} = \frac{\Delta p \, V_b}{4} \tag{2.35}$$

where N_i is the membrane force resultant, ϵ_i is the associated strain and dA_{mem} is an infinitesimal element of membrane cross sectional area.

F_{gas} is the free energy change related to isothermal expansion of the fixed N gas molecules in the microcavity. Since over the time scale of the subsequent measurements, diffusion of the gas through the SiO_x is insignificant and so number of molecules inside the cavity can be considered fixed. We compute the free energy in the gas by (V_0= Initial volume of the device).

$$Fgas = -\int P\, dV = -P_o V_o\, ln\left[\frac{Vo+V_b}{Vo}\right] \quad (2.36)$$

F_{ext} is the free energy change of the external environment that is held at a constant pressure P_{ext}. As blister expands by V_b, the volume of the surroundings decreases by an equal amount. Assuming the surroundings are maintained at the constant pressure, the free energy changes,

$$Fext = \int p_{ext} dV = p_{ext}\, V_b \quad (2.37)$$

F_{adh} is the adhesion energy between the membrane and substrate surface. For a constant value of adhesion energy per unit area Γ, so F_{adh} is (a_0: Device radius),

$$Fadh = \int \Gamma\, dA = \Gamma\, \pi(a^2 - a_0^2) \quad (2.38)$$

The constitutive equation (2.23) and along with the ideal gas equation $P_oV_0=P_{int}(V_0+V_b)$, we can use these formulas to express the free energy equation as,

$$F(a) = \frac{(Pint-Pext)\,V_b}{4} + \Gamma\,\pi(\mathrm{a}^2 - \mathrm{a}_0^2) - P_o V_o \ln\left[\frac{Vo+V_b}{Vo}\right] + p_{ext}\,V_b \qquad (2.39)$$

The first two terms represent the strain energy of membrane and separation energy between substrate and membrane respectively, and last two terms are related with isothermal expansion of the gas.

When the device is taken out from the pressure chamber, the blister expands until the free energy of the structure, *F,* reaches a local minimum. So, we minimize the free energy by taking derivative with respect to radius, *a*, and make it equal to zero, *dF/da =0.* This leads us to have the expression for the work of separation as;

$$\frac{dF(a)}{da} = -\frac{3\Delta p}{4}\frac{dV_b}{da} + \frac{V_b}{4}\frac{d\Delta p}{da} + 2\Gamma\pi a = 0 \qquad (2.40)$$

Then using the ideal gas equation, we can obtain

$$\Gamma_{\mathrm{sep}} = -\frac{5C}{4}\left(\frac{P_o V_o}{Vo+V_b(\delta,a)} - pext\right)\delta \qquad (2.41)$$

We can find Γ_{sep} of each device using the charging pressure, P_o, deflection, δ, and radius, *a,* of the blister through AFM measurements. We can also substitute the pressure term in equation (2.41) with Hencky's result in equation (2.23), we can get

$$\Gamma sep = \frac{5}{4} CKE_{2D}\left(\frac{\delta}{a}\right)^4 \qquad (2.42)$$

which is true for all devices that start to delaminate. From equation (2.42), we can determine the Γ_{sep} only using δ and *a* where we don't need to know P_o

2.4 Conclusion

This chapter reviewed theoretical part which was used to compare relevant experimental results in which we will discuss Chapter 3 and Chapter 4 of this thesis. In the next chapter, we will present the experimental work of the MoS_2/graphene heterostructure.

CHAPTER 3. STRAIN ENGINEERING: MOS_2- GRAPHENE HETEROSTRUCTURE

3.1 Introduction

Heterostructures play significant roles in modern semiconductor devices and micro/nanosystems in electronics, optoelectronics, and transducers[49]. A basic working principle of heterostructures is to use 'bandgap engineering' for manipulating carriers, for example, electrons and photons at interfaces, by leveraging the offsets in the bandgaps of different constitutive materials[23].

For experiment, we picked MoS_2/graphene structure which mediated to our ultimate goal of observing work of separation between MoS_2 and graphite.

Strain engineering is the important method which find general usage in semiconductor manufacturing. We utilize this method to improve efficiency and performance of the silicon transistors or quantum well laser[72]. Monolayer MoS_2, 2D atomic crystal, has been shown in both theory[73] and experiment[74] to be an ideal candidate for strain engineering. By tracking the A peak shift, we can predict the strain on MoS_2. Therefore, MoS_2 strain sensors are as sensitive as its silicon counterparts[75]. On the other hand, graphene has extremely high carrier mobility and zero bandgap[76]. Moreover, mechanically, graphene is extremely strong.

Materials in vdW heterostructures maintain their individual electronic properties due to the weak interactions between the layers. With the experiment, we would like to examine the interaction between MoS_2/graphene layers.

3.2 Device Fabrication

The devices are fabricated as follows. First, we started with CVD growing MoS_2 layers. To clean the SiO_x substrate before placing into furnace, we rinsed it with acetone, isopropanol and deionized water, then we kept the substrate under ultraviolet exposure for 5 minutes. A powder source of MoS_2 was placed in the center of a furnace, and SiOx substrate, which consist of 90nm thick oxidized layer, was placed in a cooler region downstream after cleaning process implementation. The furnace was pumped down to 10mTorr to remove any contaminating gases. Then we flew 60sccm Ar as a carrier gas, 0.065sccm O_2 and 1sccm H_2 gas. The furnace was heated up to 900°C and held at that temperature for 15 minutes after which it was left to cool naturally to room temperature. The process depends on the sublimation of MoS_2 at the hottest part of the furnace which is carried downstream and condenses on the substrate in a cooler region.

For the graphene growth, 25μm thick copper foils were used. Copper foils were from Alfa Aesar and didn't have any coating on the surface. Foils were rinsed with acetone, isopropanol, and deionized water as it was done in MoS_2 growth. Then, copper foils were placed middle of the furnace. The furnace was pumped down to low pressure around 76mTorr and we sent the 14sccm CH_4 as a carbon resource, and 7sccm H_2. Yield and quality of CVD graphene are directly related with C:H ratio[77] and smoothing the surface of copper foil[78]. H_2 was kept flowing all the process but CH_4 was only turned on during the growth stage which is 15 minutes. The furnace was heated to 1000°C and after growing period it was left to cool naturally to room temperature.

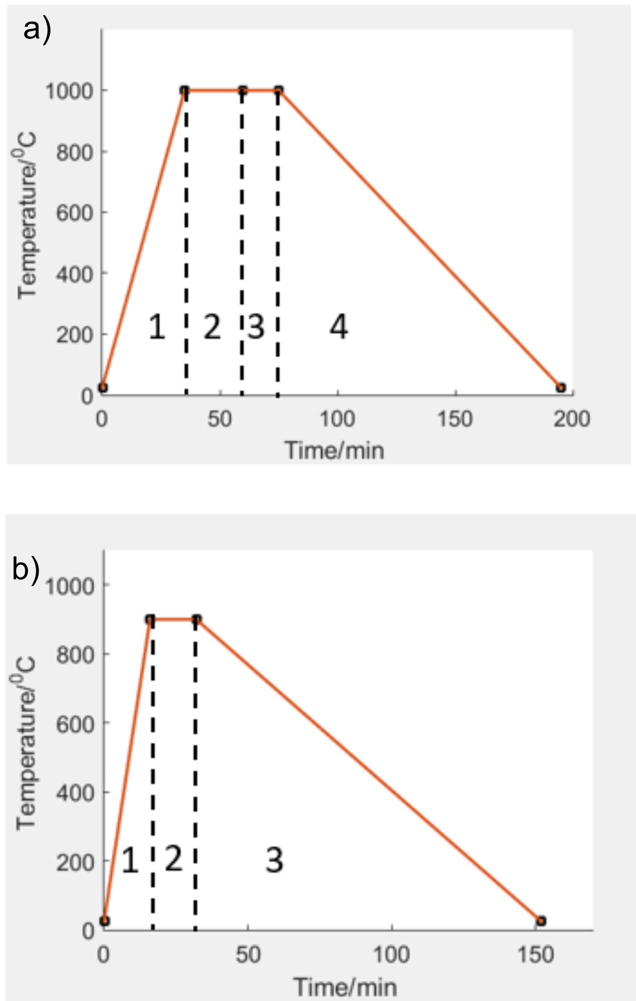

Figure 3.1. a) Schematic figure of the time elapse during CVD graphene growth. Zone1: heat ramping stage. Only H_2 is allowed to flow and heated up to 1000ºC. Zone2: Pre-annealing area. Zone3: Growth period which we start to send CH_4. Zone4: Cooling stage. b) Schematic figure of the time elapse during CVD MoS_2 growth. Zone1: Heat ramping stage. H_2, O_2, Ar are sent this stage. Zone2: Growth stage. Zone3: Cooling stage

The etched holes were prepared before we started to transfer process. SiO_x wafer was covered with S1818 photoresist solution and exposed to UV for 17.5

seconds under the mask which the mask has 5μm holes that were imprinted on it. Right after this process, Reactive Ion Etching(RIE) was applied under oxygen, sulfur hexafluoride (SF_6) and tetrafluoromethane (CF_4) medium to etch through the Si and SiO_x. Typically, we obtained *~5μm* diameter and *~800-950 nm* depth holes. For removing photoresist completely, we put the wafers into 'Remover 1165' for over 12 hours at 105°C and then oxygen plasma was applied respectively.

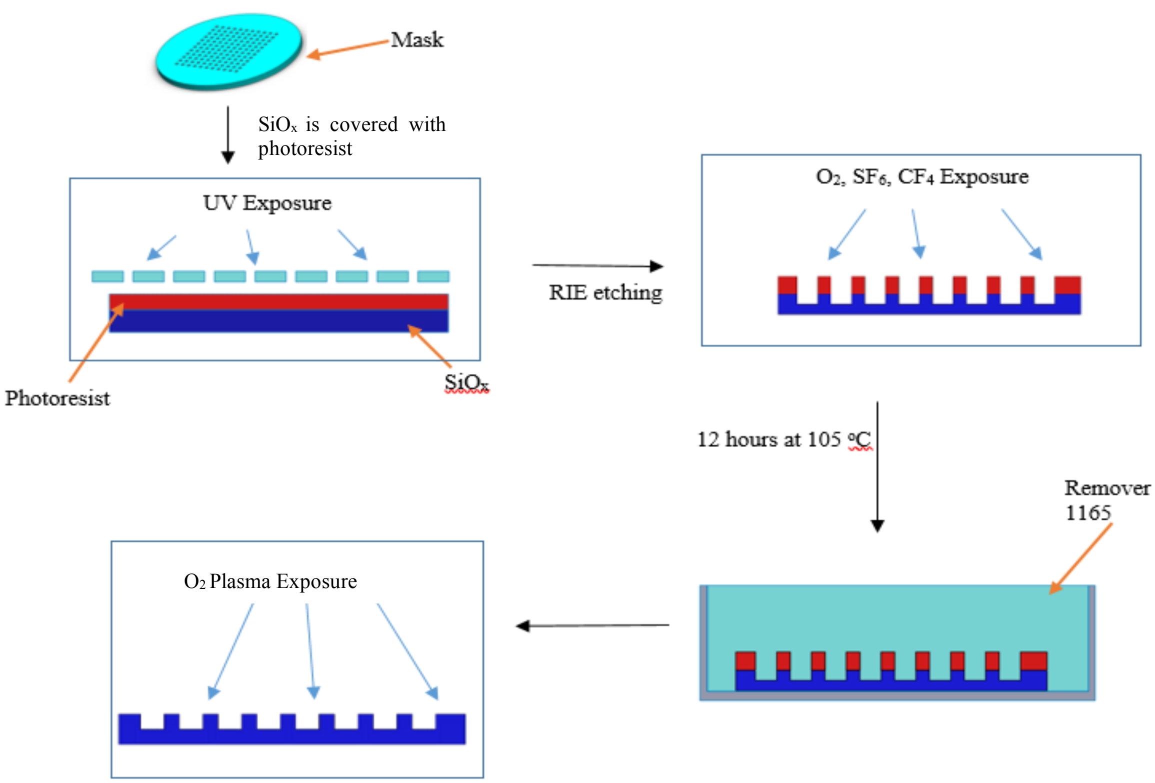

Figure 3.2. Schematic of SiO_x holes preparation

After successfully finishing the 2D materials growths, MoS_2 layer was covered with Polymethyl methacrylate (PMMA) for transferring onto pre-etched cavities. Following to this process, thermorelease frame was put on to PMMA surface, then placed into deionized(DI) water for peeling off the MoS_2. Before annealing off the PMMA layer at 340°C, the devices were left in a vacuum desiccator for > 2 days to allow any gas trapped in the microcavities to leak out.

For graphene, before we covered it with PMMA, one side of the copper foil was exposed to oxygen plasma for 5 minutes to remove graphene growth at that one side. After completing PMMA coverage process, as it performed in MoS_2 transfer, thermorelease frame was put onto PMMA-covered side and then copper underneath was etched thoroughly. The concentration of the etchant was *DI water/Etchant= 5/1*. Graphene-PMMA layer was transferred to annealed MoS_2 which was taken from the desiccator after 2 days. Then another annealing process was run at the same conditions. The schematic of the fabrication process is depicted below.

a) MoS_2 Growth

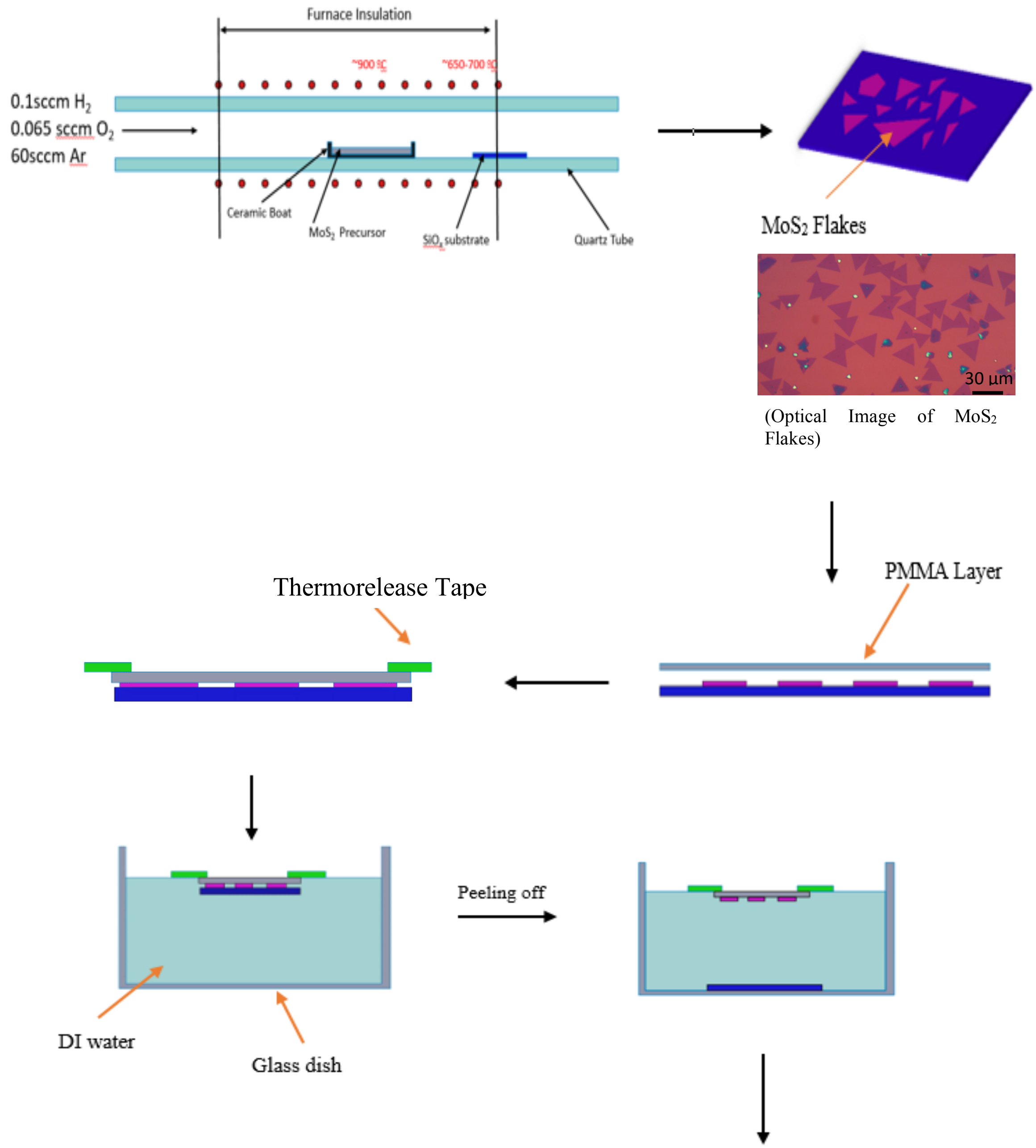

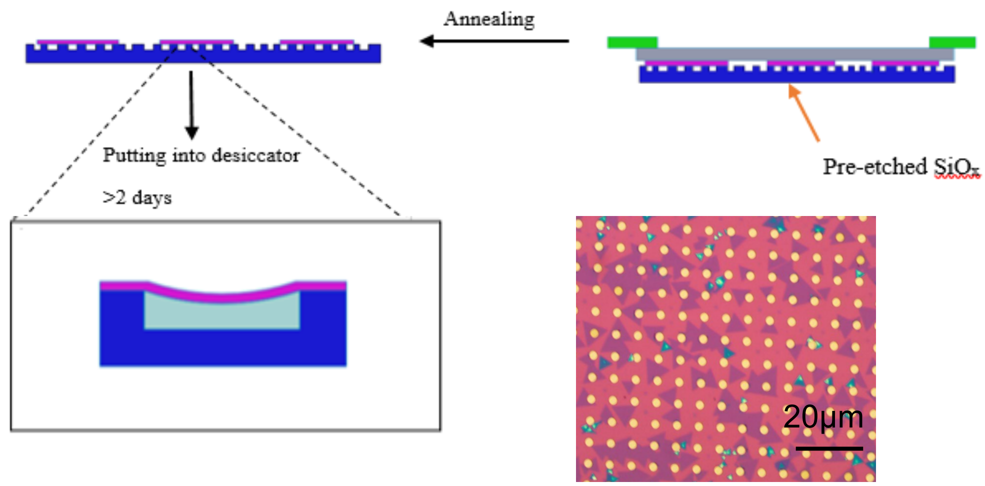

b) Graphene Growth

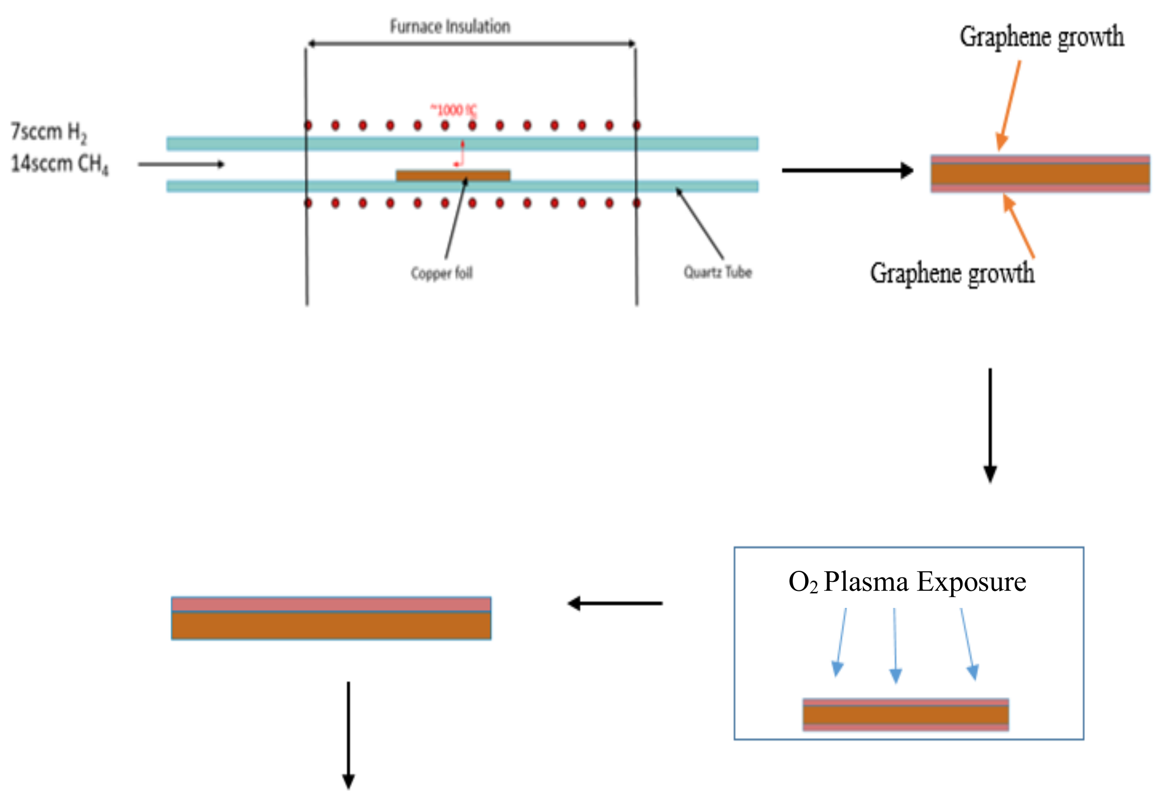

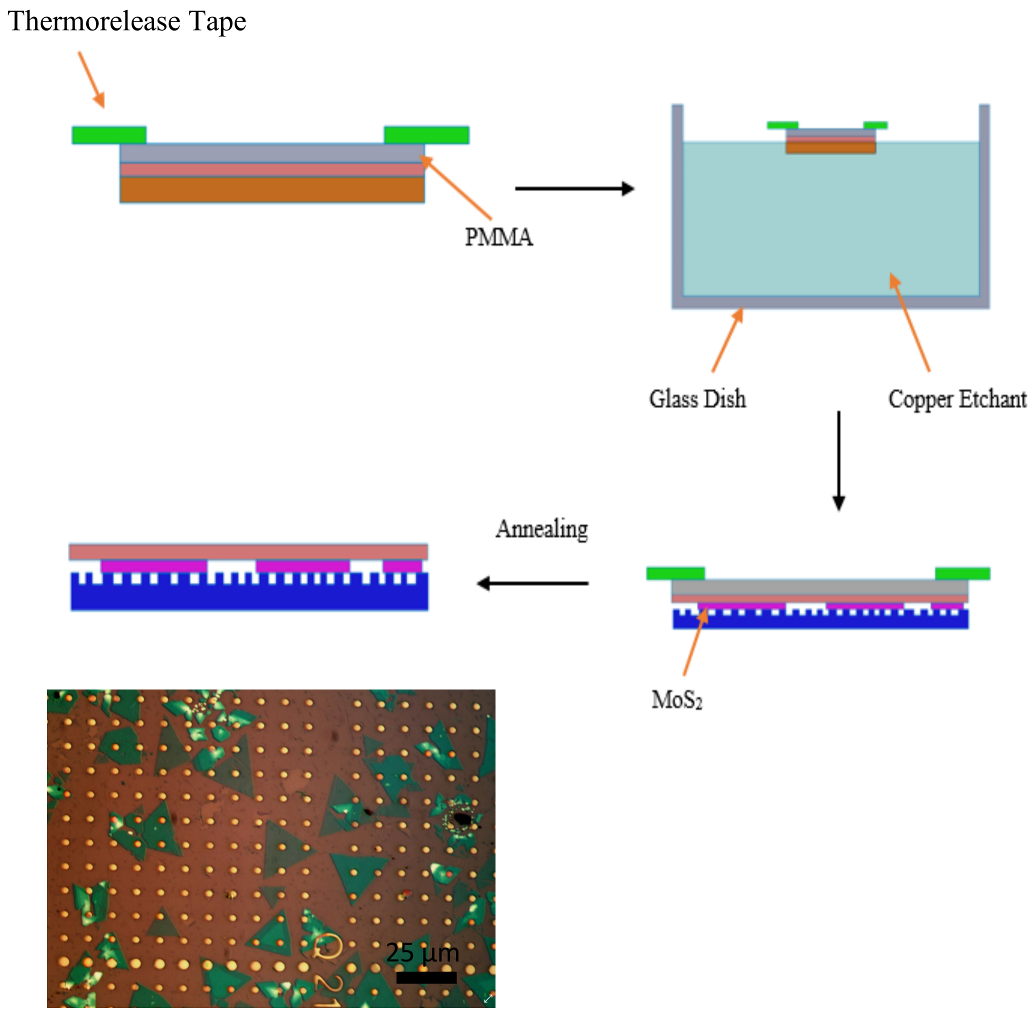

Figure 3.3. Schematic of 2D Heterostructure Preparation

3.3 Device Characterization – AFM and Raman

A tapping mode AFM was used to measure the diameter and depth of the etched wells before we transfer anything on to it. All AFM scans were taken using Dimension 3100 operating in ambient conditions.

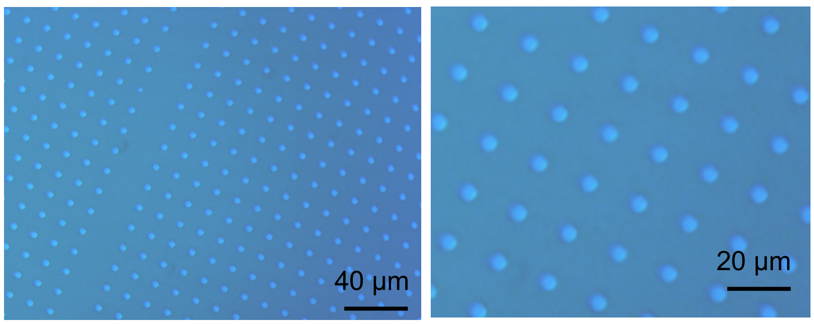

Figure 3.4. ~5µm etched holes on SiO_x

Before we start to fabricate heterostructure, we checked the Raman spectroscopy and Photoluminescence(PL) of our 2D materials individually to be sure about their growth quality. For this purpose, we used a Renishaw InVia Raman microscope, laser with a wavelength of 532nm that was focused on the material via *100x* objective. Each measurement was performed within *40 seconds* and *28.3µW* power was used. The grating was picked as *1200 l/mm*.

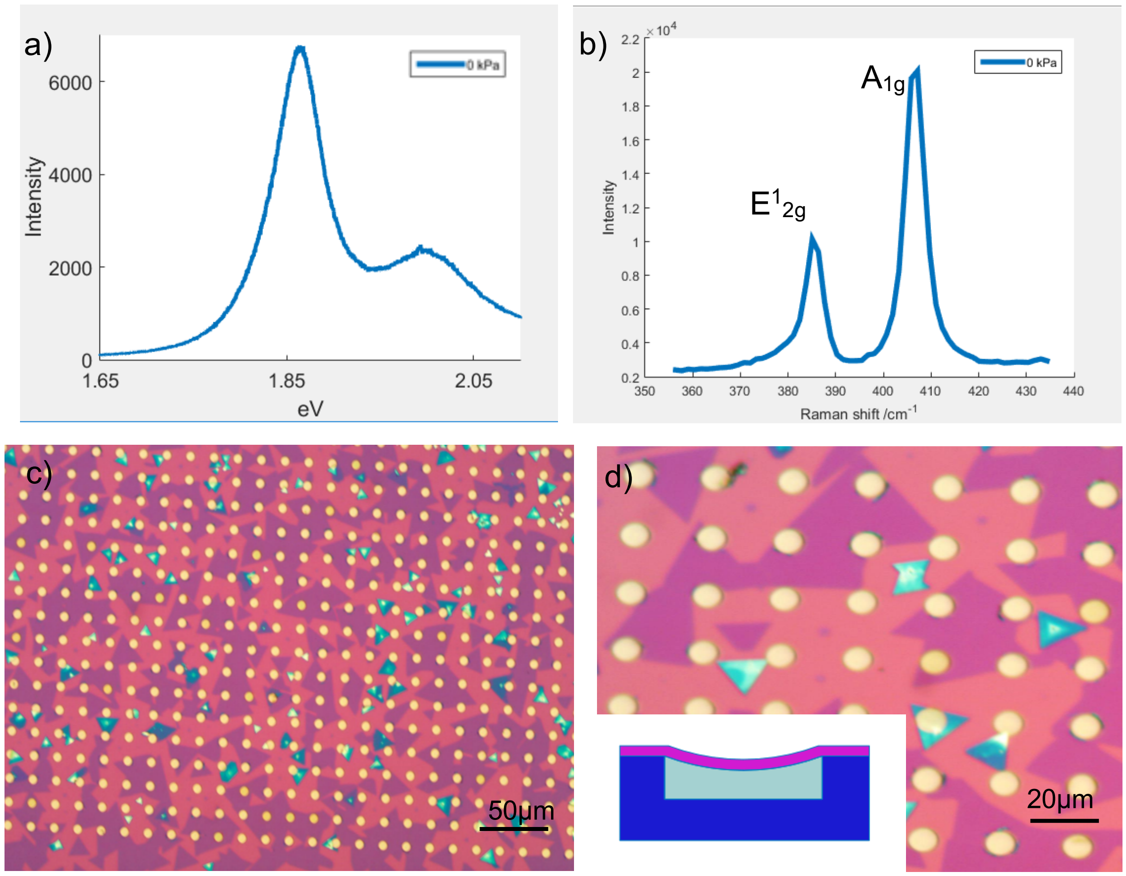

Figure 3.5. a) PL measurement of CVD growth MoS_2 b) Raman spectroscopy of CVD-growth MoS_2 c) Microscope image of MoS_2 on the wells d) Zoomed image of MoS_2 wells (Inset: Schematic image of MoS_2 on the wells after taking out from desiccator.)

Also we obtained the graphene Raman spectroscopy in addition to this study to be sure that we obtained monolayer graphene from CVD method.

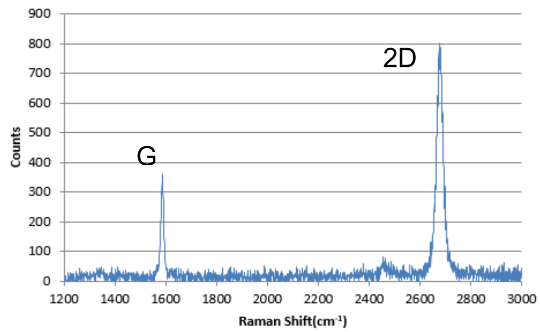

Figure 3.6. a) Raman spectroscopy of CVD growth graphene

After fabricating the heterostructure, we measured the Raman spectroscopy of device to be sure about presence of the both layers over the holes. Furthermore, we ran Raman during experiment because it is possible that the device could get broken when we introduce higher pressure and we wanted to track the peaks shifts as well.

In Figure 3.7., we were able to see the corresponding peaks of the graphene and MoS_2. Intensity of the signals were increased for the graphene peaks due to presence of the doping which stemmed from strain residues during transfer and the MoS_2 straining[81,82,83], as well as CVD growth graphene naturally have higher intensities than pristine graphene which are obtained by exfoliation method.

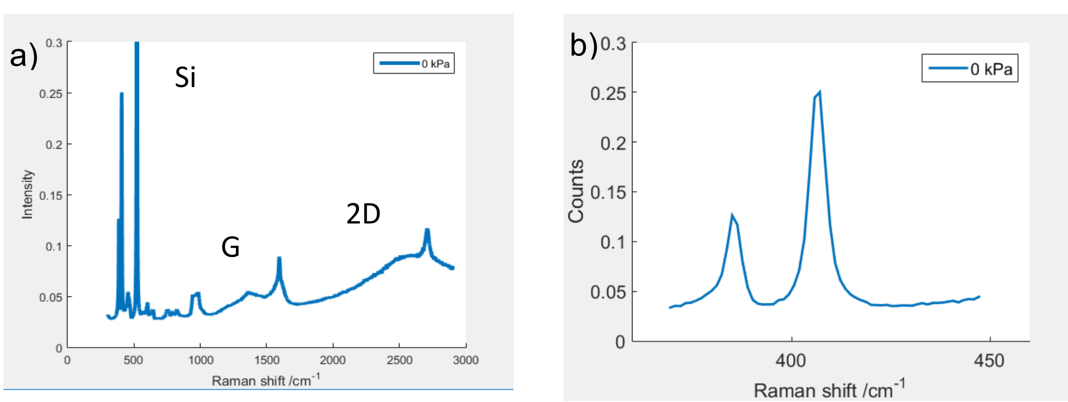

Figure 3.7. a) Raman Spectroscopy of heterostructure. b) Zoomed in area of MoS_2 peaks

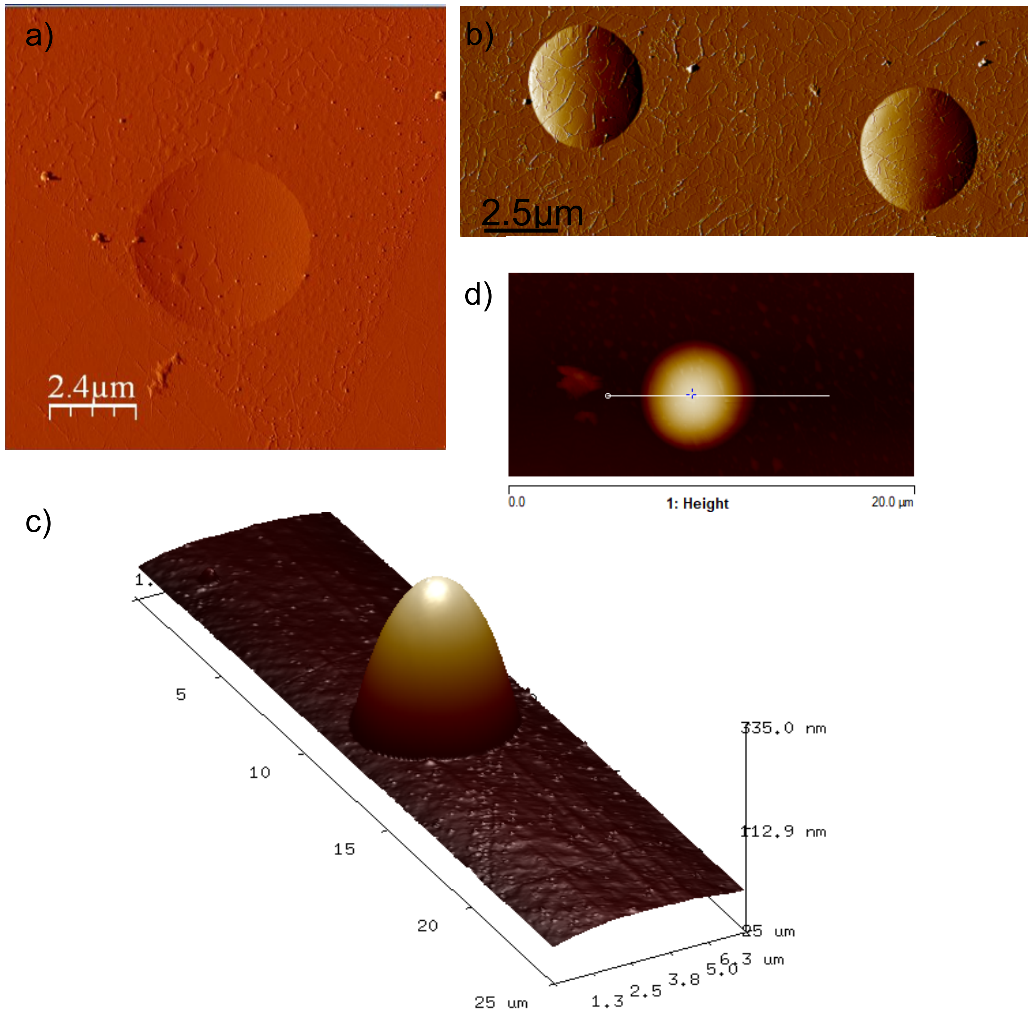

Figure 3.8. a) AFM image of suspended heterostructure before pressurizing b) AFM image of the bulged up devices c) 3D image of the one of the devices d) Obtaining the cross-section for each device to find out maximum deflection.

3.4 Data Analysis

3.4.1 Strain Analysis

The devices were placed into a pressure chamber and pressure was set to the P_0. We let the device stay in the chamber more than one and half day because we wanted gas to leak into the cavities through the SiO_x substrate. After one and half day, the internal pressure, P_{int}, and P_o became equal ($P_{int} = P_0$). This process is illustrated in Figure 3.9. We used Ar for charging gas because Ar leaks out so slow which is the biggest advantage for us because we would have enough time to finish measurements, and within these times the change in the deflection is so small that was in the allowable range for our calculation. When the devices were taken out from the pressure chamber the P_{int} was greater than the external pressure ($P_{ext} = 1\ atm$), and this pressure difference ($\Delta p = P_{int} - P_{ext} > 0$) forced the membrane to bulge up. For each charging pressure, P_0, we measured the deflection, δ, and radius, a, of the blister using an AFM and took Raman measurements, respectively. Then, device was placed back pressure chamber to set higher charging pressure.

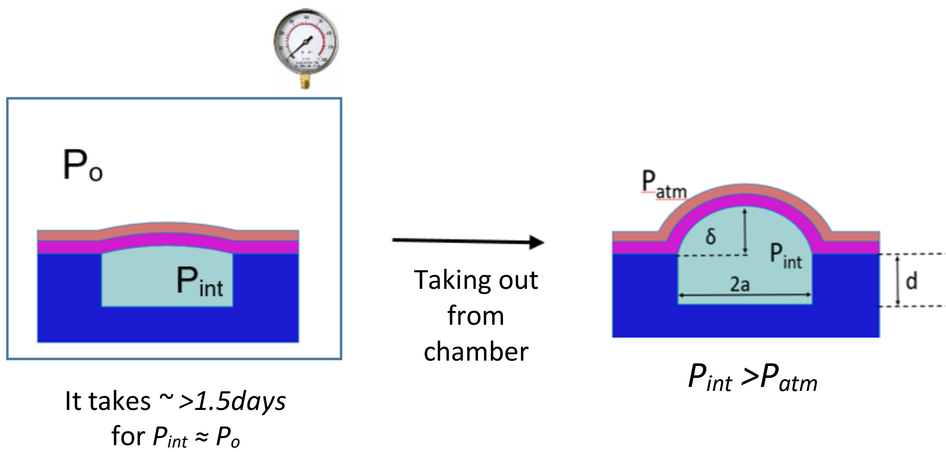

Figure 3.9. Diagram of Blister Test Process of MoS_2/graphene Heterostructure

After determining the deflection and radius values for each charging pressure with help of the AFM, we were able to calculate the biaxial strain by using the formula

$$\varepsilon_b = \left(\frac{\delta}{a}\right)^2 \frac{(1-\nu)B_0\, K(\nu)^{2/3}}{4} \tag{3.1}$$

the Poisson's ratio was taken *0.29* [41]. Equation (3.1) was discussed in Chapter 2, so constants were found as $K(v=0.29) = 3.54$ and $B_0 = 1.72$

Along with the AFM scanning, we also took the PL spectrum for each charging pressure. As it mentioned at the chapter 1, the band gap of the MoS_2 changes ~100 meV/% for biaxial strain[41]. Therefore, we calculated the strain by converting the PL peak positions. Since we know the biaxial strain for each charging pressure, we associated these values with the PL positions of the corresponding pressure charging, and they were plotted in fig 3.10.

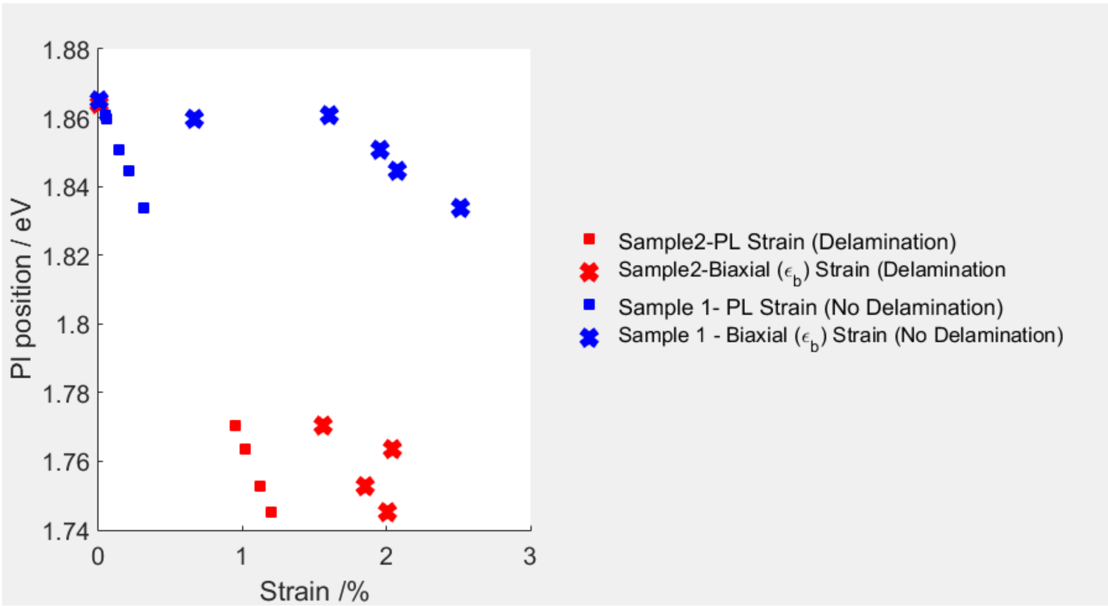

Figure 3.10. Comparison between the biaxial strain and PL converted strain.

One easy comment on the Figure 3.10 can be said that there is mismatch between the strains. We were expecting to observe that biaxial strain values would have been in the range of the PL strain but biaxial strain turned out to be higher due to the crumpling on the graphene membrane[84].

In Figure 3.11. and Figure 3.12. we plotted the two examined devices' Raman spectroscopy and PL measurement. For the further analysis, we compared their E^1_{2g}, A_{1g}, *2D,* and *G* peak shifts. Strain change affects the graphene's *2D* peaks more than *G* peak[84]. It is also observable at Figure 3.13a-b, *2D* peak and *G* peak of the graphene for sample 1 shifted more drastically than the sample 2 because sample 1 had good conformity between its layers. Since we fitted our data to linear line, we wanted to find the 'Gruneisen' parameter of the graphene in the heterostructure. We used the formula[95];

$$\frac{\Delta w_{G;2D}}{w^0_{G;2D}} = -2\,\gamma_{G;2D^{\varepsilon}} \quad (3.2)$$

where $\Delta w_{G;2D}$ is change rate of the either peaks, and $\gamma_{G;2D}{}^{\varepsilon}$ is the Gruneisen parameter. If we use this formula to calculate the corresponding Gruneisen parameter for our case, we would have the values for both *G* and *2D* parameters that are off by the magnitude of 0.002 from the previous study[95]. We observed the deviation because of the crumpling on graphene.

Table 3.1. Gruneisen Parameter Calculation

Method	Υ_G	Υ_{2D}
Blister[95]	1.8	2.4
From Measured Data	$3.58 * 10^{-3}$	$4.69 * 10^{-3}$
Ratio (Exp/Blister)	0.002	0.002

Furthermore, for sample 2, there was sliding occurrence between the layers of graphene and MoS_2. We can understand this phenomenon by again tracking the corresponding graphene Raman peak shifts related to strain change which was caused by pressure difference[96]. On the other hand, if we follow the MoS_2 Raman peaks we can conclude that peaks stayed roughly where they started due to biaxial strain[41]. As it is seen at the Figure 3.11a and 3.12a, the band gap changed accordingly to change in strain. PL intensities didn't show consistent decrease because each measurement had been performed in different time so this has direct effect on the intensities. However, we needed to keep track on the peaks' positions which were in agreement with previous study[41].

<u>Sample 1</u>

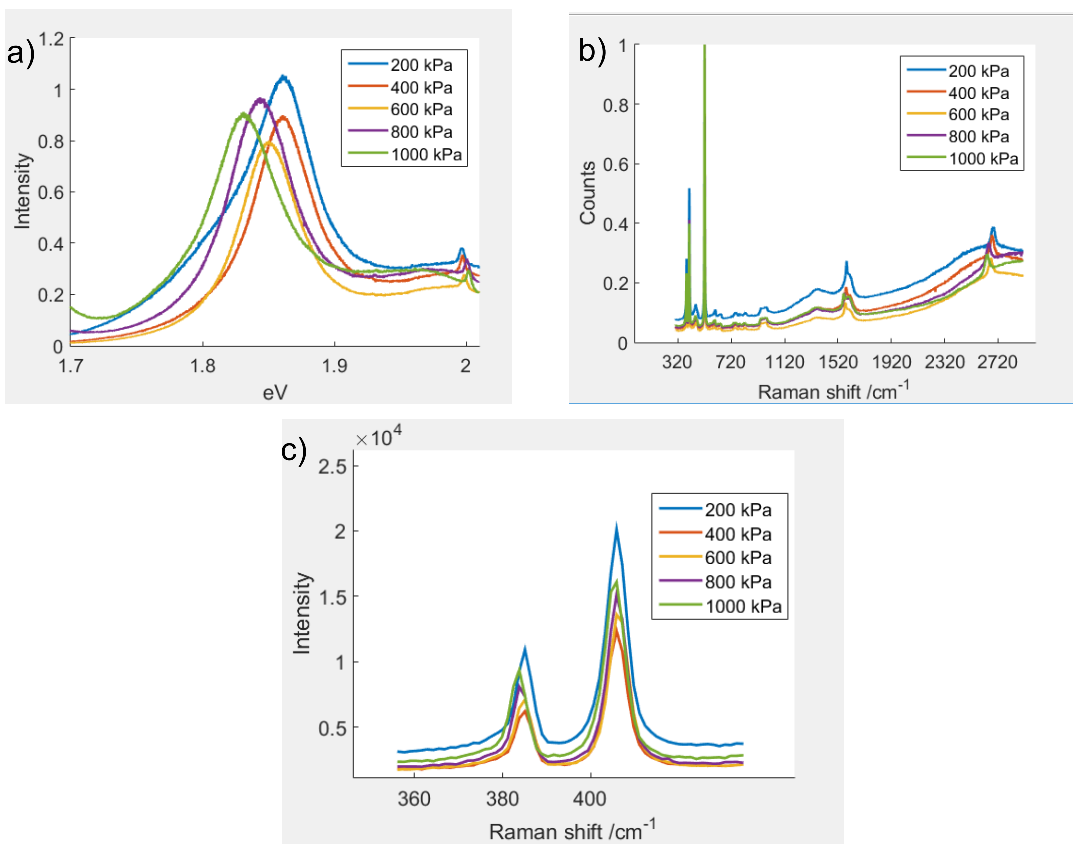

Figure 3.11. All these plots were depicted for Sample 1 a) PL measurement of heterostructure. (normalized with Si peak) b) Raman spectroscopy. (normalized with Si peak) c) Raman peaks of MoS_2.

Sample 2

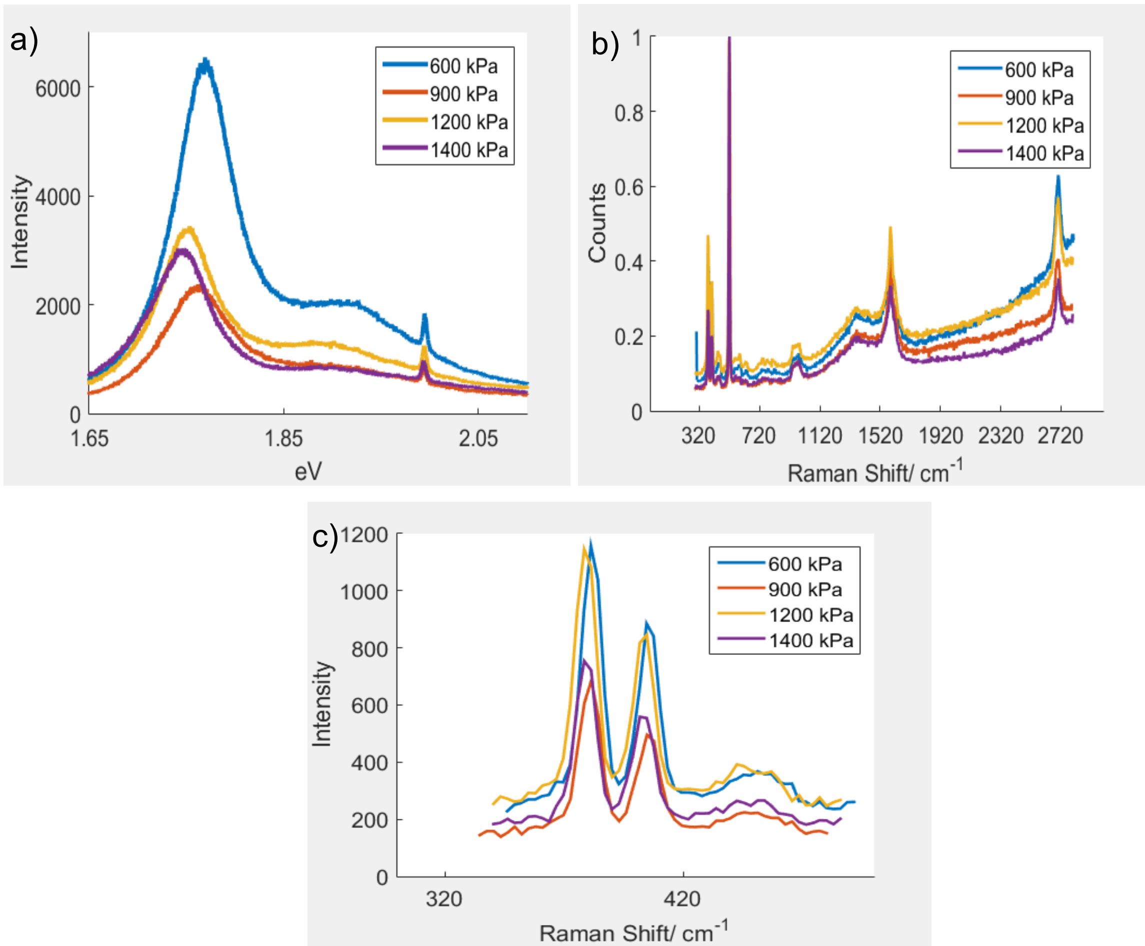

Figure 3.12. All these plots were depicted for Sample 2 a) PL measurement of heterostructure. b) Raman spectroscopy. (normalized with Si peak) c) Raman peaks of MoS_2.

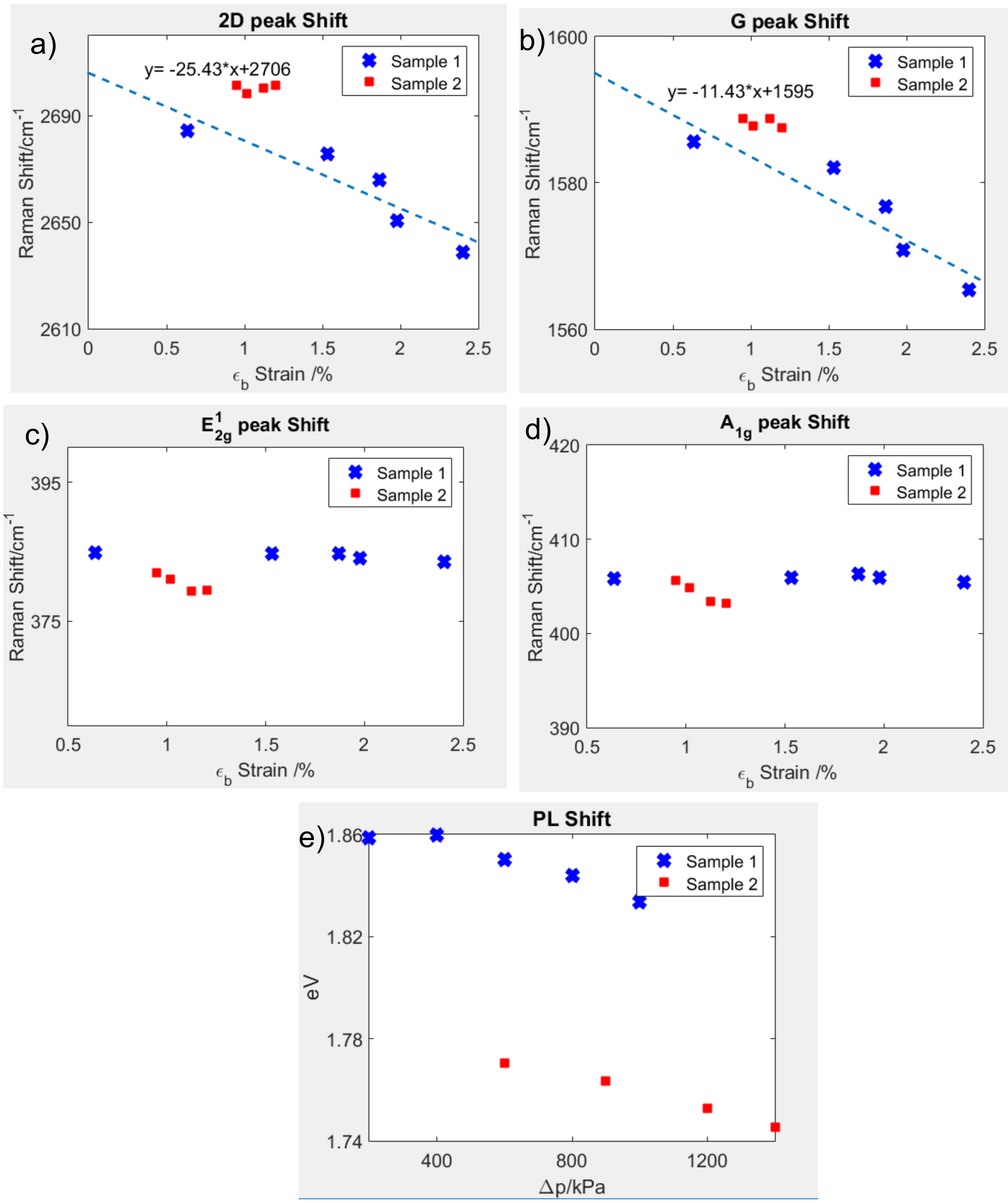

Figure 3.13. a) *2D* peak shift comparison (Dashed line is linear fit for Sample 1) b) *G* peak shift comparison (Dashed line is linear fit for Sample 1) c) E^1_{2g} comparison d) A_{1g} comparison e) PL shift comparison

Moreover, we fabricated 2 more devices in addition to Sample 1 and Sample 2 but they didn't withstand the higher pressure difference. However, we include their PL data to plot PL shift change in low strain area. In Figure 3.14., it can be easily seen, there are PL shift jumps occurrence at the lower strain. We attributed this phenomenon that due to conformity between the MoS_2/graphene layer, MoS_2 gets the shape of the crumpling graphene so during the pressure increase, layer becomes flat and this flatness causes shift jumps in the PL spectroscopy.

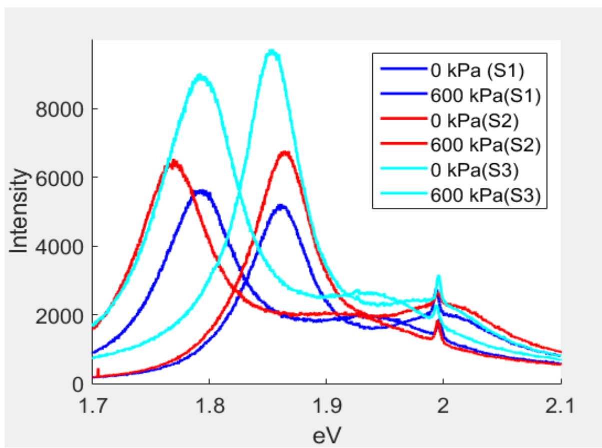

Figure 3.14. PL shifts at low strain area (S1: Sample1 etc.)

Even when there is no pressure difference across the membrane there is usually a residual pre-strain observed in suspended devices, due either to the transfer procedure or the membrane sticking to the sidewalls of the cavity[22]. PL spectroscopy can be used to estimate the pre-tension in our membranes.

Obtaining PL measurement of our device at zero pressure difference and computing corresponding strain value, we can convert this to a pre-tension value by using the formula

$$\sigma_0 = \frac{E_{2D}\varepsilon_0}{1-v} \tag{3.3}$$

Our devices had a pre-strain of ε_0 *~0.002* and corresponding stress is *~0.37 N/m*. In the Camplbell's[85] study, it was shown that we can utilize the non-dimensional parameter which is given below.

$$P = \frac{\Delta p \ a \ E_{2D}^{1/2}}{\sigma_o^{3/2}} \tag{3.4}$$

If the $P>100$, Hencky's formula in equation (2.25) is correct to within *5%*. $P = 100$ when $\Delta p = 350kPa$. Since nearly all of our data was taken with $\Delta p > 350kPa$. Hence, we can neglect the effect of the pre-tension.

3.4.2 Work of Separation – Graphene/MoS_2 on SiO_x

As it can be seen in Figure 3.15., increase in P_0 causes δ to increase. Initially, membrane remains pinned at the radius of the microcavity, a_0. After a critical pressure is reached; it is supposed to start delamination because the pressure difference across the membrane exceeds therefore adhesion force can't keep the membrane clamped to the surface. In our experiment we only observed this for just one device. First, by using the values of δ, and a we will determine E_{2D} for both devices, and we will use E_{2D} while calculating the work of separation. We used the equation (2.25) and plotted it against the pressure difference between pressure inside the cavity and atmospheric pressure. The inverse of the slope gave us the E_{2D} (Figure 3.16.). The average value of the E_{2D} was found as *115 N/m*. In addition to that, we calculated the theoretical Young's modulus of the heterostructure by using following formulas[49]

$$t_{hetero} = t_{Gr} + 0.65nm \quad (3.5)$$

$$E_{Hetero} * t_{hetero} = E_{Gr} * t_{Gr} + E_{MoS2} * t_{MoS2} \quad (3.6)$$

where t_{Gr} was taken 0.355 nm[94], and 0,65 is MoS_2 thickness[49]. Combining equation (3.5) and equation (3.6), the Young's modulus of the heterostructure is given by;

$$E_{Hetero} = E_{Gr} - (E_{Gr} - E_{MoS2}) * (0.65\ nm / t_{Gr} + 0.65nm) \quad (3.7)$$

For this calculation we used E_{Gr} = *340 N/m* [98] and E_{MoS_2} =*160 N/m*[106].

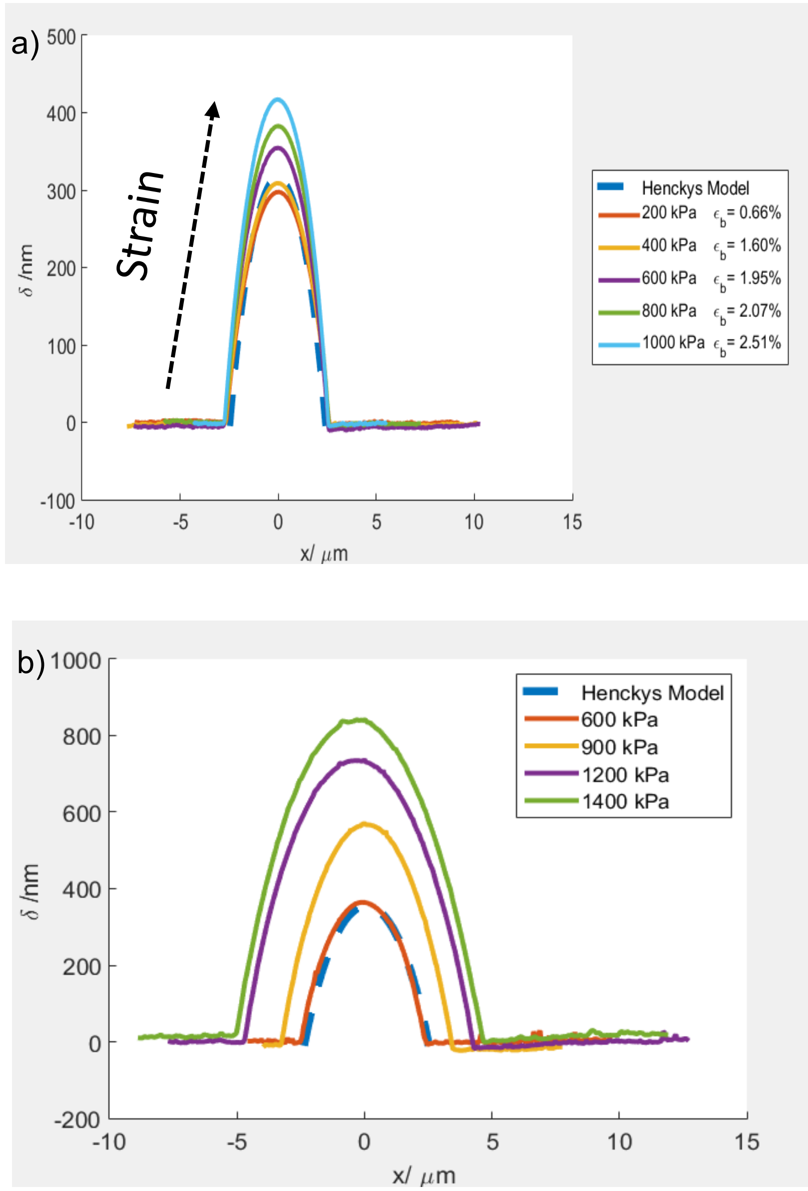

Figure 3.15. a) Deflection of Sample 1 at varying Δp. No delamination is observed b) Deflection of Sample 2 at varying Δp. Delamination is observed.

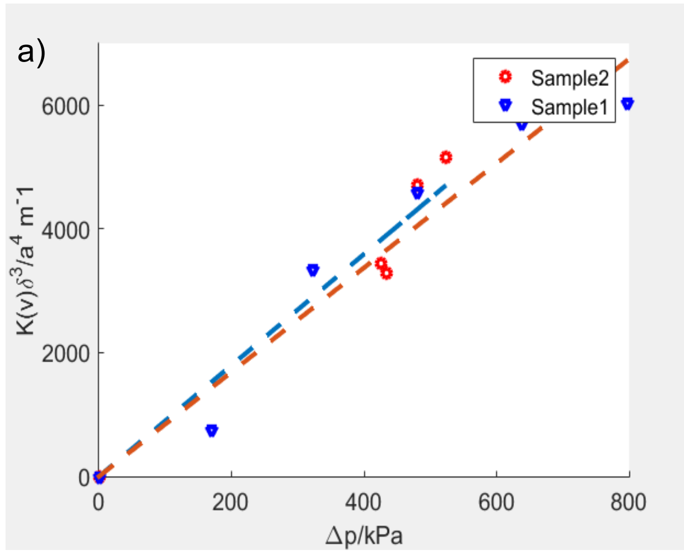

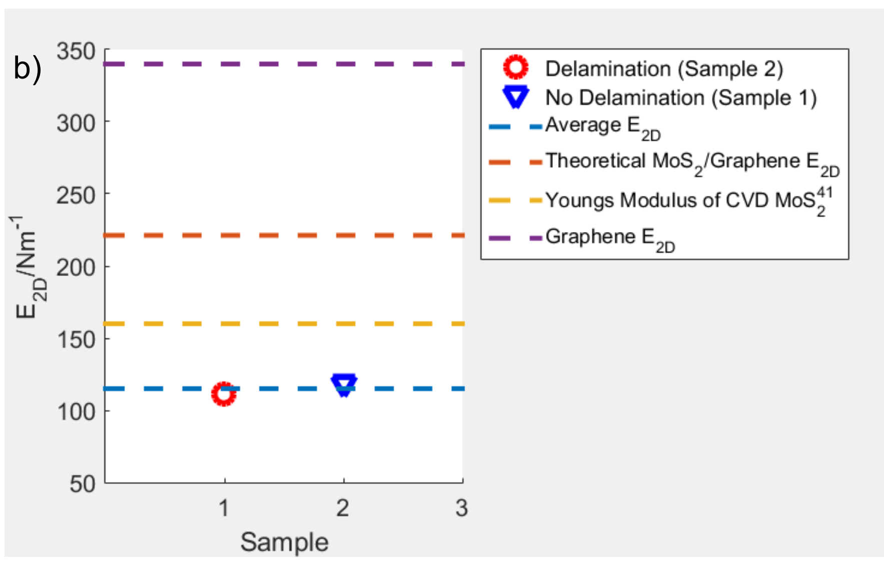

Figure 3.16. a) Plot for heterostructure devices used to determine E_{2D} (data fitted linearly (dashed lines)) b) Theoretical and experimental E_{2D} calculations

Due to wrinkles on the graphene, it caused to lose its stiffness [84]. By looking Fig. 3.16b, we conclude that crumpling causes so much softening on the material.

Finally, we used the calculated Young's modulus for each device to measure the work of separation. We used the formula which was deduced previously;

$$\Gamma sep = \frac{5}{4} CKE_{2D} \left(\frac{\delta}{a}\right)^4 \quad (3.8)$$

The mean value of separation energy of these two device was found as $\Gamma_{sep} \geq 201\ mJ/m^2$. The delaminated device fit into the range of that was found by Lloyd et al.[106] MoS_2 on the SiO_x. However, the device which showed no delamination has higher work of separation. The possible explanation for that during the transfer of MoS_2 on to surface, some hydrocarbons might trap between the substrate and layer that affected the separation energy [86].

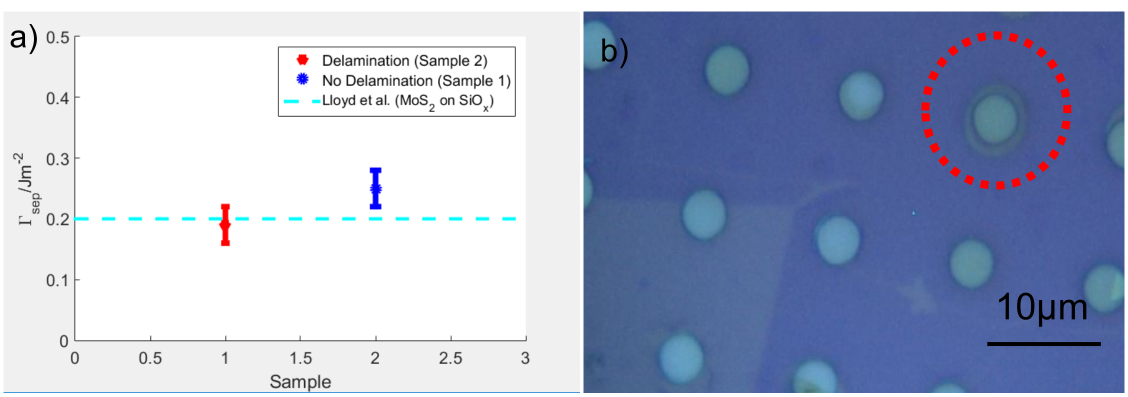

Figure 3.17. a) Work of separation of heterostructures. b) Delaminated device (red circle)

3.5 Conclusion

In conclusion, we fabricated two bilayer heterostructure devices which consist of monolayer graphene and MoS_2. We placed them into pressure chamber to create pressure difference between the cavity and atmosphere to cause them to bulge up. By means of the AFM, we were able to measure deflection and radius of the membranes. Along with the AFM measurement, we ran the Raman spectroscopy at the center of the bubbles which had the highest deflection. First, we calculated the strain by using geometrical inputs which we obtained from AFM and by using PL shifts of the MoS_2. We observed that there is a mismatch between the biaxial and PL strain values. We attributed that to graphene crumpling, as a consequence of crumpling, we observed softening at the stiffness. Second, we took the AFM data and used for determining separation energy calculation. The device which showed delamination had separation energy is closer to values of previous studies. On the other hand, non-delaminated showed higher separation energy is greater or equal to $0.26 Jm^{-2}$. Further experiments are needed in order to verify our results more precisely.

CHAPTER 4. MoS_2 ON THE GRAPHITE HOLES

4.1 Introduction

Two-dimensional (2D) materials are promising nanomechanical structures[2]. Understanding the interaction between the heterostructure is important which opens unprecedented possibilities for various technological applications. The heterostructural formed semiconductors constitute a majority portion of the modern semiconductor industry[87]. We can vertically stack 2D layers by mechanically transferring them top of each other which is a fast and convenient way of fabricating heterostructures.

Graphene has already produced a vast number of offspring across many classes of materials. Graphene seems a suitable material to combine with alternative vdW solids due to its lack of dangling bonds, chemical inertness, and the ability to remain intact under high stress.

Furthermore, monolayer MoS_2 shows great mechanical properties[88] along with being piezoelectric[89], and has a direct band gap which is highly sensitive to strain changes[90].

A good understanding of adhesion between the materials therefore draws researchers' attention to create effective and precise applications. Because, the performance of the devices is directly related to adhesive and tensile forces involving the material growth quality. Adhesive force is important parameter for determining the maximum strain of 2D materials can withstand, besides we should take into consideration if we would like to design stretchable electronic devices[91] and pressure sensors[91]. Since we know from the scotch tape method that we are able to create smooth graphite surfaces. Therefore, we etch the holes through the exfoliated graphite flakes and transfer the single MoS_2 layer over the holes to study work of separation between the MoS_2 and graphite.

4.2 Device Fabrication

MoS_2 was prepared and transferred onto wells as the same way where it is described in chapter 3. Only difference was occurred the preparation of the target substrate which specifically for this experiment is graphite holes. First, we rinsed the SiO_x substrate with acetone, isopropanol, and DI water. Then the graphite flakes were placed onto substrate by Scotch tape method. Following this, we covered surface with S1818 photoresist solution and exposed it to UV for *17.5sec*. Right after this process, Reactive Ion Etching (RIE) was applied under oxygen, and tetrafluoromethane (CF_4) medium to etch through the graphite and SiO_x. Typically, we obtained *~5 μm* diameter and *~450-650nm* depth for graphite + SiO_x holes. To be sure about removing photoresist completely, we put the wafer into acetone for over *12 hours at 55^{o}C*. One of our aims was also to control the whether any treatment on the surface makes a difference on the separation energy. For this purpose, the surface was exposed with the oxygen and the argon, then the MoS_2 was transferred over the wells. By using this fabrication method, we made 6 separate devices. Before annealing the PMMA after MoS_2 transfer, we put the devices into a desiccator for >2 days for making sure any gas trapped inside could leak out. After this process, devices were placed into the pressure chamber to create pressure difference which caused deflection on the membrane.

Graphite hole preparation

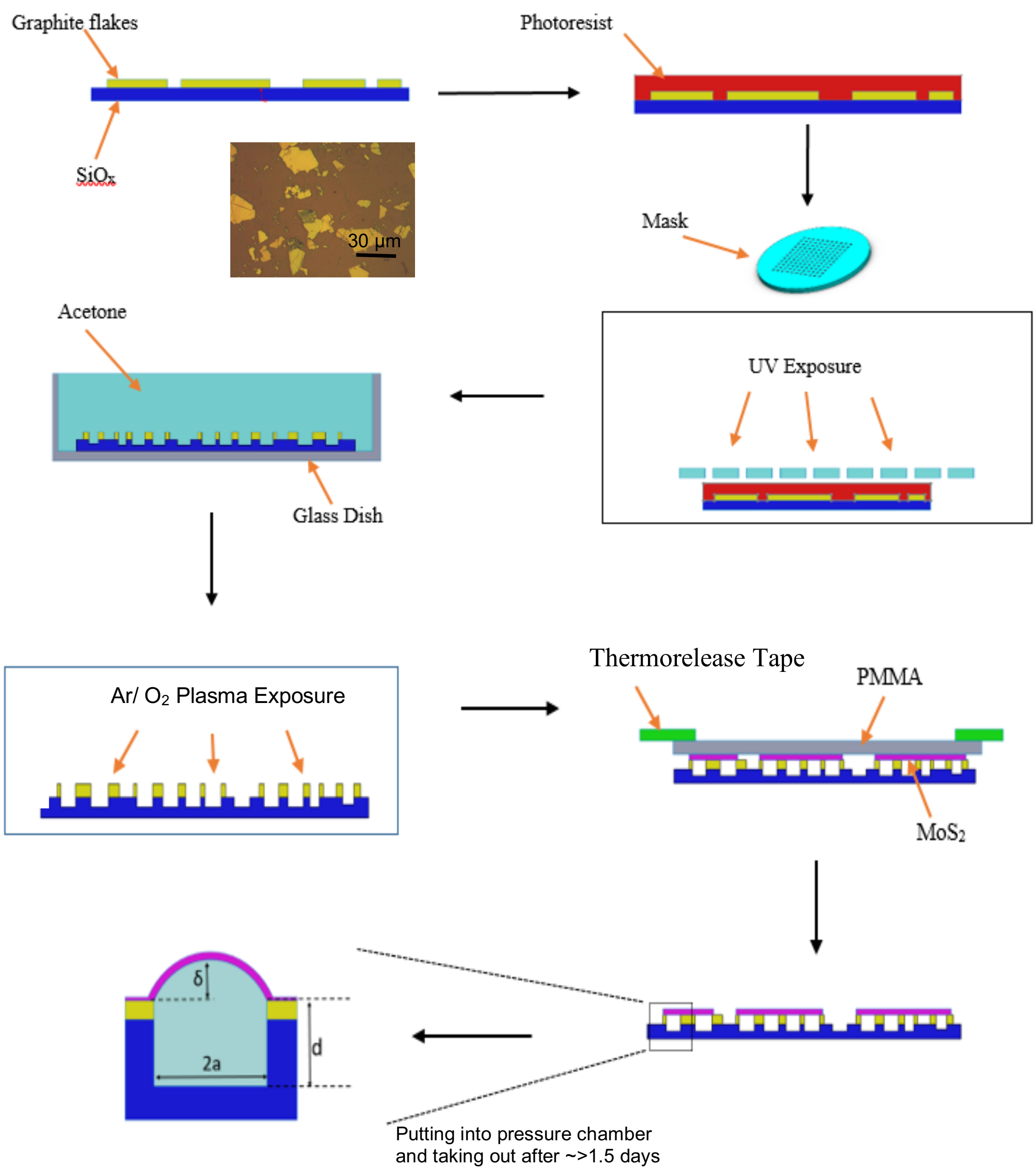

Figure 4.1. Preparation of Graphite hole and MoS_2 transfer process

4.3 Device Characterization – AFM and Raman Spectroscopy

Again tapping mode AFM was used to measure the diameter and depth of the etched wells before starting transfer process. All AFM scans were taken using Dimension 3100 operating in ambient conditions using silicon cantilevers.

We used the MoS_2 from the same batch which was growth previously, therefore it had the same Raman and PL properties. Before we start to transfer the MoS_2 on to the wells, optical microscope was used to control the any photoresist residues remain at the surfaces.

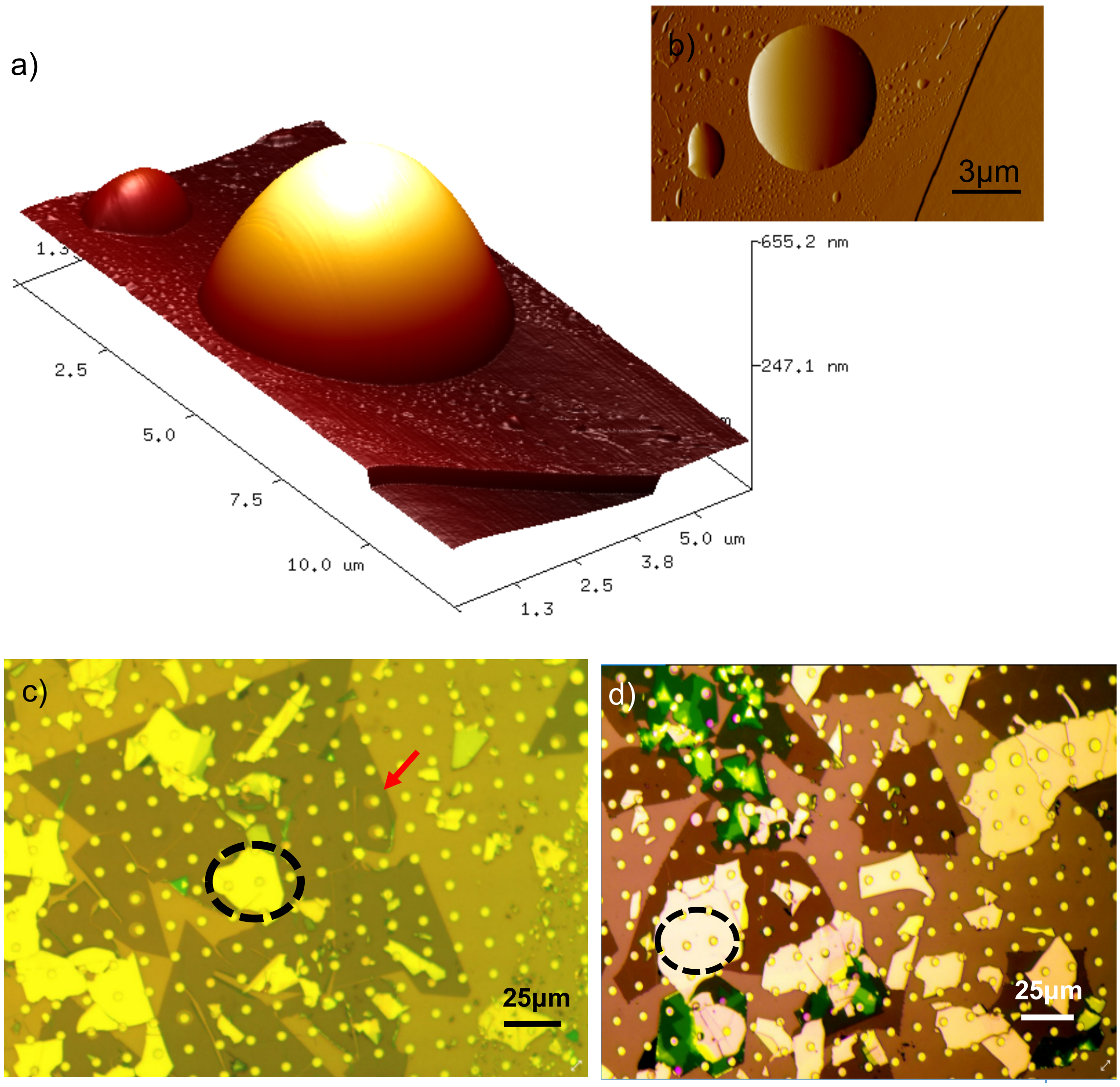

Figure 4.2. a) 3D image of the MoS_2 on the graphite holes. b) AFM image of the MoS_2 on the graphite hole. c)Optical microscope image of the MoS_2 on the SiO_x areas shows delamination (red arrow shows the delaminated area, black circle indicates the measured area.) d) Optical microscope image of another device we fabricated and measured (black circle indicates the measured area.)

4.4 Work of Separation – MoS_2 on Graphite Holes

Before placing our 6 devices into pressure chamber, we took the PL measurement of the MoS_2 to confirm that pre-strain and corresponding stress are in the limit which they don't affect the results. To determine that, we used the same approach what we discussed for the vdW heterostructure in previous chapter. According to this approach, we took most of our data above the *400kPa*.

The devices were placed into a pressure chamber filled with Ar of pressure P_0. We kept them in the pressure chamber more than one and half day to reach equilibrium. For every cycle of the increasing the pressure, we did the same thing. When the devices were taken out of the chamber, the difference between the inside the cavity and atmospheric pressure caused deflection on the membrane. Every cycle of the process, we measured the deflection, δ, and radius of the blister with AFM. We used Hencky's model to described the deformation of the membrane. In Figure 4.3., we plotted the AFM result and Hencky's solution. It is clear that Hencky's model fits to our experimental data perfectly.

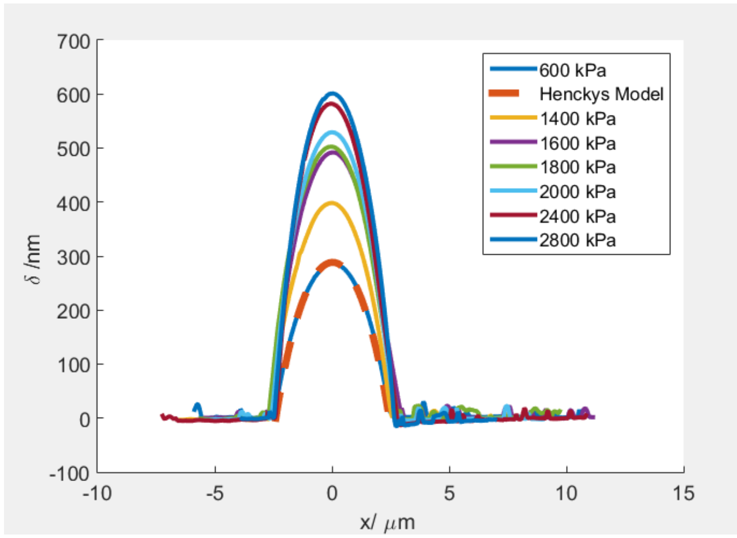

Figure 4.3. AFM cross section corresponding pressure charge. We plotted Hencky's model which is in agreement with our experimental data.

Then using the AFM results, we calculated the E_{2D} of the devices by using the equation (2.25) and plotted it against the pressure difference between pressure inside the cavity and atmospheric pressure. By looking the Figure 4.4. the average E_{2D} is equal to *147 N/m* which is within the same range of previously found value[92].

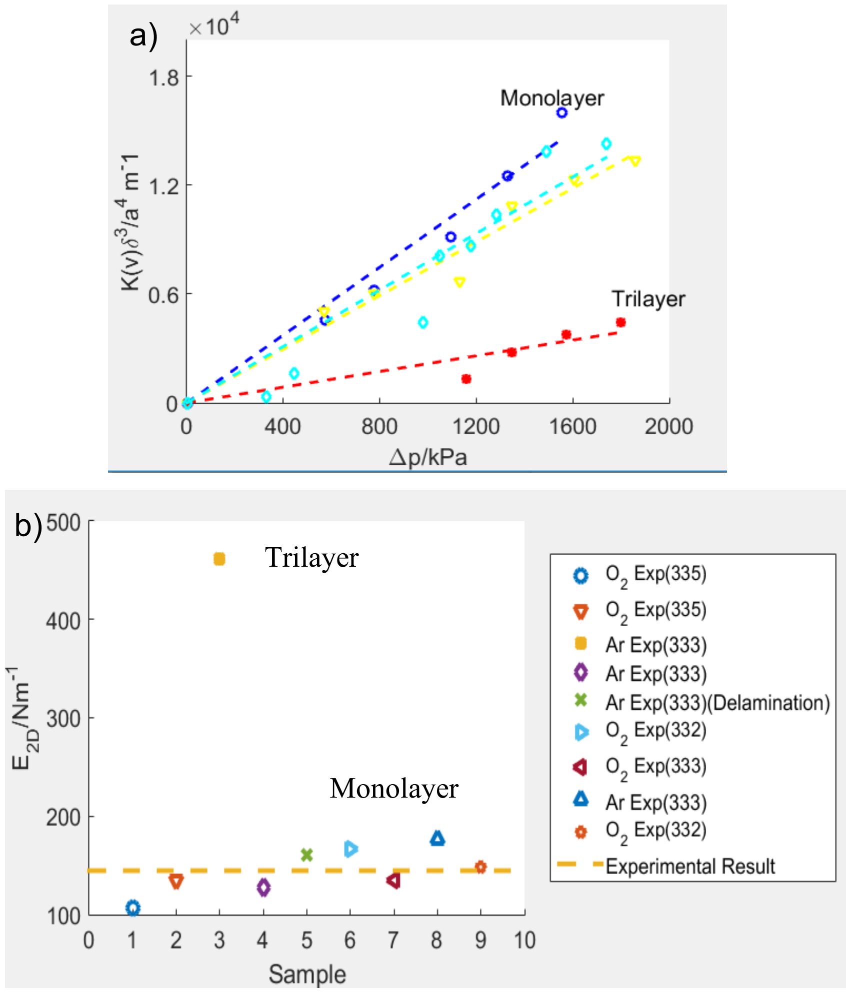

Figure 4.4. a) Plot for calculating E_{2D} for CVD monolayer and trilayer MoS_2 devices (data fitted linearly (dashed lines)) b) We compiled all devices we measured. In legend, it is specified for each device how they were exposed with corresponding gas written nearby with encoded recipes. (For example; Ar Exp (335) = Argon exposed with 300mW power, 300sccm and 5min). Experimental result indicates that we obtained monolayer MoS_2.

Next, we determined the work of separation, using the AFM results and free energy formula which is described in Chapter 2. Only one of our devices has shown the delamination. If we look the Figure 4.5., we can conclude that the separation energy is higher at graphite surface where MoS_2 layers were located on the SiO_x

substrate. From calculation of separation energy is equal or greater than 320 mJ/m^2. Values on the blue box which the devices are located on the SiO_x substrate show agreement with study of Lloyd et al.[106]

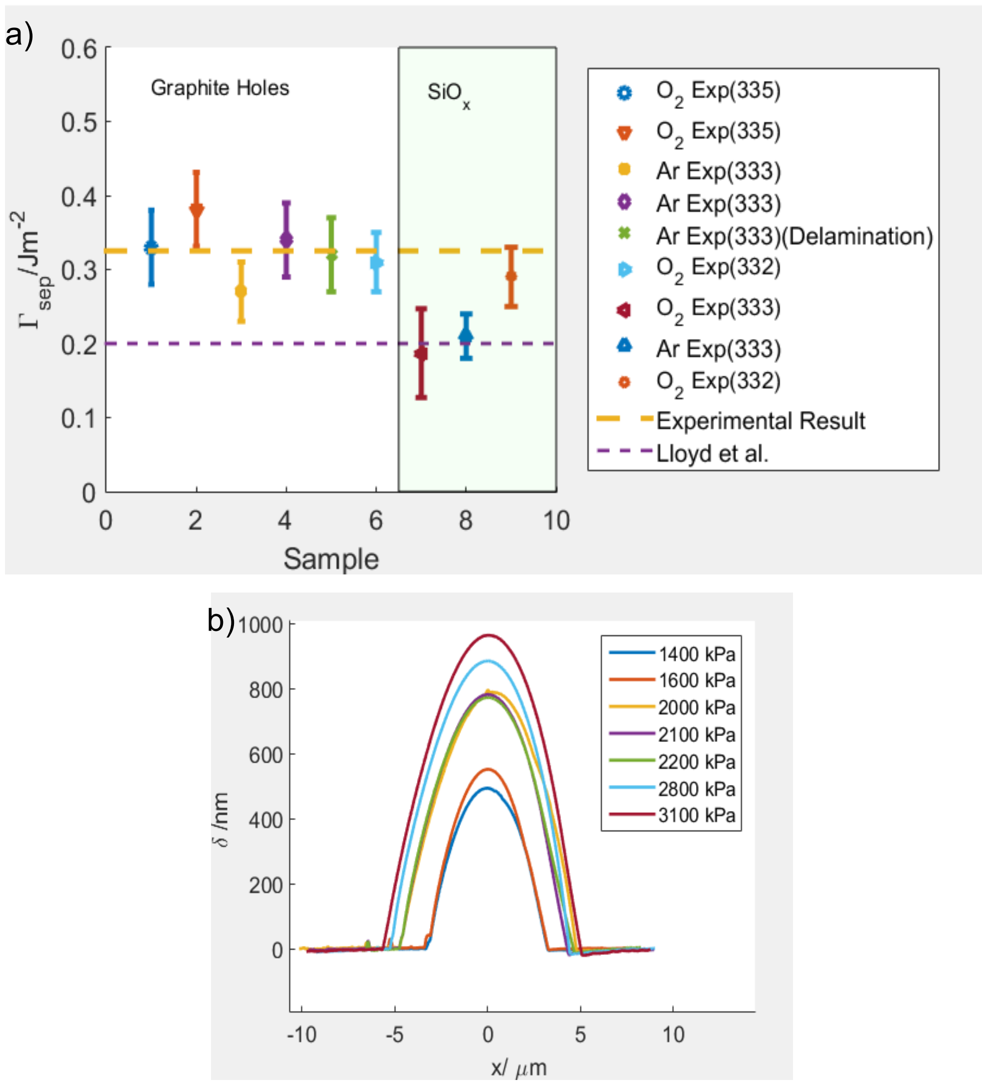

Figure 4.5. a) 6 devices outside the blue box are on the graphite hole. Only one of them showed delamination during experiment. On the other hand, the measured areas have the same separation energy. The devices in blue box are located on the SiO_x which are in agreement with previous study. b) Plot of the deflection of the delaminated device.

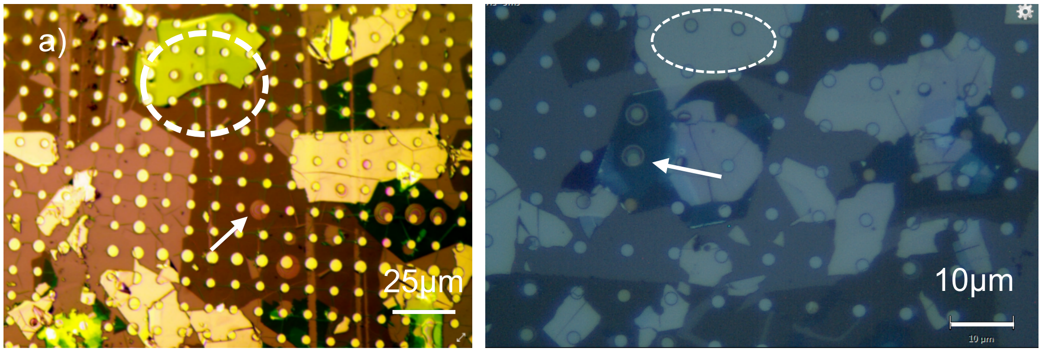

Figure 4.6. a) and b) are the optical images of the devices. White circles indicate the area where we did measurement. Arrows show the delamination.

We also wanted to find the critical pressure which we were expecting to see starting of the delamination for corresponding separation energy. Figure 4.7. clearly shows the devices not following the local minima in the free energy. Our devices have pinned at same radius in which it originally started except one. This means that we have higher separation energy than measured one.

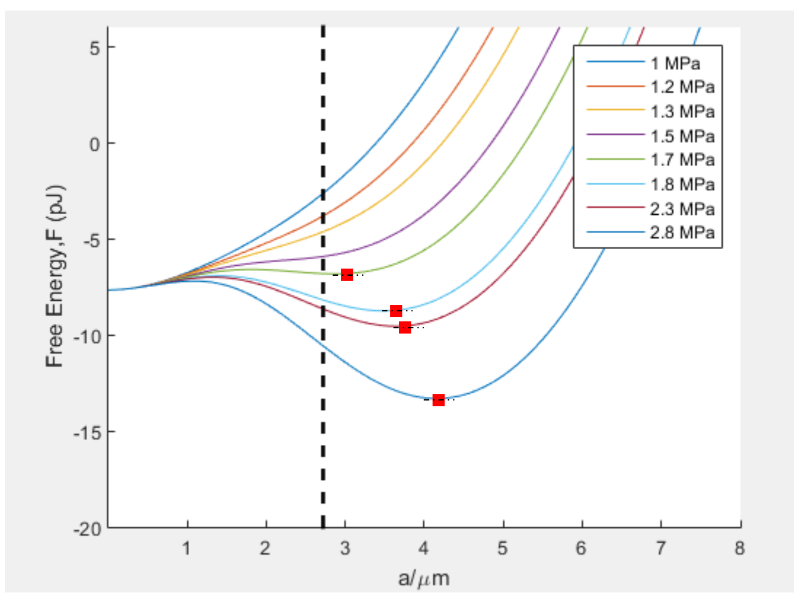

Figure 4.7. The free energy landscape. Black dashed line indicates the edge of the hole. Red squares the local minima for corresponding charging pressure.

4.5 Conclusion

In this chapter, we created graphite holes, then we transferred MoS_2 on to these holes. To be able to measure work of separation, we put them into the pressure chamber to introduce pressure difference between the cavity and the external pressure which is atmospheric pressure. Every pressure charging, we measured the deflection and radius by using AFM. Only the one device showed delamination within the 6 device. By means of thermodynamic model, we calculated the separation energy is great or equal to 320mJ/m^2, which is higher than MoS_2 on the SiO_x. However, further works are needed to be sure whether there is a delamination occurrence at higher pressures. With this experiment we can conclude that the difference in separation energy between the 2D materials affects the performance of nanomechanical heterostructural devices[93].

CHAPTER 5. CONCLUSIONS

5.1 Summary

This thesis explored mechanical properties of the 2D vdW heterostructural materials and work of separation. Chapter 1-2 included an overview of the basic concepts and the theoretical explanations and the experimental results presented in chapter 3-4. Chapter 1 began by introducing the intrinsic properties of the graphene and graphite and continued with MoS_2 as well as explaining the Raman spectroscopy and AFM measurement. Chapter 2 provided an introduction to the theory which we utilized to compare our experimental results.

The experimental section started in Chapter 3. We created MoS_2/graphene bilayer and transferred it on to the SiO_x wells. Then by changing the pressure inside the cavity, we calculated the strain changes by using results obtained from AFM measurements against PL shifts obtained from Raman microscopy. These experiments demonstrated that there is mismatch between values of the strains which we attributed this to feature of the graphene. Because CVD growth monolayer graphene shows crumpling. This phenomenon also leads to decrease the stiffness of the bilayer heterostructure.

In chapter 4, we fabricated graphite holes to measure the separation energy to compare with the previous studies. For this purpose, we etched holes ~5μm holes through the graphite flake which were exfoliated onto the SiO_x substrate. Then MoS_2 transferred on to wells. The same approach also followed in here. We placed 6 devices into pressure chambers to cause them bulge up to measure deflection and radii. From the experimental results, we found that the separation energy is higher than MoS_2 on the SiO_x wells. Even at the very high pressures (~2700 kPa) MoS_2 layers on the graphite wells stayed pinned to same diameter where they originally started.

5.2 Future Outlook

There are still many new and interesting problems related to interaction between 2D heterostructure. We grew atomically thin membranes by CVD method that are highly impermeable to gases and can withstand large pressure differences. However, the presence of various defects has great effect on the mechanical properties of 2D materials. We should also study and carry out further experiments to understand the interplaying properties of the 2D heterostructure in addition to the van der Waals interaction. Moreover, the effects of surface roughness and capillary bridging effects are the other factors that are need to be studied.

As it was shown in Chapter 4, the adhesive forces are important to shape the mechanical behavior of atomically thin materials. The blister and the other adhesion experiments need to be done with other 2D materials such as h-BN, WSe_2 etc. Toward to explaining the separation energy between the various 2D heterostructure, our experiment gives the promising results. There are also unanswered questions still exist. For example, performing the blister test on rectangular or square membrane could lead different results which has never been tried yet. Also studying how the heterostructural layers slide with respect to each other is another vital point that needs to be touched by researchers to contribute to understanding of the interplay between the layers more clearly.

With finding the new methods of fabricating the heterostructures along with the transferring methods will increase the quality of the devices. Providing good quality of material all over the device for large scale is still main challenge. With the advent of the new methods, we could comprehend the fundamental factors ruling behind heterostructures more precisely. There are also other issues about controlling defects, and understanding the effect of the substrates that need to be addressed.

2D heterostructures open a new research field and with the advancing in this field we would have novel devices with desired properties. Predictably, the further progresses in 2D material growth, heterostructure device fabrication, more precise band gap alignments, and defining the other interplaying forces would ease to have higher quality devices and lead us set up more practical applications in near future.

REFERENCES

[1] A.K. Geim, K.S. Novoselov, “The rise of graphene”, *Nature Materials, 6(3)*,183–191, March 2007.

[2] K.S. Novoselov, D. Jiang, F. Schedin, T.J.Booth, V.V. Khotkevich, S.V. Morozov and A. K. Geim, “Two-dimensional atomic crystals”, *Proceedings of the National Academy of Sciences of the United States of America*, 102(30),10451-10453, July 2005.

[3] D. Pierucci, H. Henck, J. Avila, A. Balan, C.H. Naylor, G. Patriarche, Y.J. Dappe, M.G. Silly, F. Sirotti, A.T.C. Johnson, M.C. Asensio, A. Ouerghi, “Band Alignment and Minigaps in Monolayer MoS_2-Graphene van der Waals Heterostructures”, *Nano Letters*, 16(7), 4054-4061, June 2016.

[4] K.S. Novoselov, A. K. Geim, S.V. Morozov, D. Jiang, Y. Zhang, S.V. Dubonos, I.V. Grigorieva, A.A. Firsov, “Electric Field Effect in Atomically Thin Carbon Films”, *Science*, 306(5696), 666-669, October 2004.

[5] T. Li, “Ideal strength and phonon instability in single-layer MoS_2”, *Physical Review B*, 85:235407, June 2012.

[6] Y. Sun, S.E. Thompson, T. Nishida, “Physics of strain effects in semiconductors and metal-oxide-semiconductor field-effect transistors”, *Journal of Applied Physics*, 101:104503 May 2007.

[7] T. Zhu, J. Li, “Ultra-Strength Materials”, *Progress in Materials Science*, 55(7), 710-757, April 2010.

[8] R.M. Yunus, H. Endo, M. Tsujj, H. Ago, “Vertical heterostructures of MoS_2 and graphene nanoribbons grown by two-step chemical vapor deposition for high-gain photodetectors”, *Physical Chemistry Chemical Physics*, 17:25210, September 2015.

[9] S.P. Koenig, N.G. Boddeti, M.L. Dunn, J.S. Bunch, “Ultrastrong adhesion of graphene membranes”, *Nature Nanotechnology*, 6(9), 543-546, August 2011.

[10] E. Stolyarova, K.T. Rim, S. Ryu, J. Maultzsch, P. Kim, L.E. Brus, T.F. Heinz, M.S. Hybertsen, G.W. Flynn, “High-resolution scanning tunneling microscopy imaging of mesoscopic graphene sheets on an insulating

surface”, *Proceedings of the National Academy of Sciences of the United States of America*, 104(22), 9209-9212, May 2007.

[11] K.S. Novoselov, “Beyond the wonder material”, *Physics World*, 22(08):27, August 2009.

[12] J.C. Meyer, A.K. Geim, M.I. Katsnelson, K.S. Novoselov, T.J. Booth, S. Roth, “The structure of suspended graphene sheets”, *Nature*, 446(7131),60-63 March 2007.

[13] A.K. Geim, I.V. Grigorieva, “Van der Waals heterostructures”, *Nature*, 499(7459), 419–425, July 2013.

[14] M. Dienwiebel, G.S. Verhoeven, N. Pradeep, J.W.M. Frenken, J.A. Heimberg, H.W. Zandbergen, "Superlubricity of Graphite", *Physical Review Letters*, 92(12):126101, March 2004.

[15] P. R. Wallace, “The Band Theory of Graphite”, *Physical Review*, 71(9), 622-634, May 1947.

[16] I.V. Gornyi, V.Y. Kachorovskii, A.D. Mirlin, “Anomalous Hooke’s law in disordered graphene”, *2D Materials, 4*(1): 011003, 2017.

[17] A.K. Geim, K.S. Novoselov, “Graphene”, *Royal Swedish Academy of Sciences*, The Nobel Prize in Physics 2010, (http://www.nobelprize.org/nobel_prizes/physics/laureates/2010/advanced.html)

[18] G.N. Dash, S.R. Pattanaik, S. Behera, “Graphene for electron devices: The Panorama of a decade”, *IEEE Journal of the Electron Devices Society*, 2(5), 77-104, September 2014.

[19] F. Bonaccorso, Z. Sun, T. Hasan, A.C. Ferrari, “Graphene photonics and optoelectronics”, *Nature Photonics*, 4,611–622, September 2010.

[20] C. Lee, X. Wei, J.W. Kysar, J. Hone, “Measurement of the Elastic Properties and Intrinsic Strength of Monolayer Graphene”, *Science*, 321(5887),385-388, July 2008.

[21] D. Jiang, R. Cooper, S. Dai, “Porous Graphene as the Ultimate Membrane for Gas Separation”, *Nano Letters*, 9(12), 4019-4024, September 2009.

[22] J.S. Bunch, S.S. Verbridge, J. S. Alden, A. M. van der Zande, J. M. Parpia, H.G. Craighead, P.L. McEuan, “Impermeable atomic membranes from graphene sheets”, *Nano Letters*, 8(8), 2458-2462, August 2008.

[23] K.S. Novoselov, A. Mishchenko, A. Carvalho, A.H. Castro Neto, “2D materials and van der Waals heterostructures”, *Science*, 353(6298):aac9439, July 2016.

[24] P. Blake, E.W. Hill, K.S. Novoselov, A.H. Castro Neto, D. Jiang, R. Yang, T.J. Booth, A.K. Geim, “Making graphene visible”, *Applied Physics Letters,* 91:063124, April 2007.

[25] N.I. Kovtyukhova, Y. Wang, A. Berkdemir, R. Cruz-Silva, M. Terrones, V. H. Crespi, T.E. Mallouk. “Non-oxidative intercalation and exfoliation of graphite by Brønsted acids”, *Nature Chemistry*, 6(11), 957-963, November 2014.

[26] C. Riedl, C. Coletti, T. Iwasaki, A. A. Zakharov, U. Starke, “Quasi-Free-Standing Epitaxial Graphene on SiC Obtained by Hydrogen Intercalation”, *Physical Review Letters*, 103(24):246804, December 2009.

[27] C. Berger, Z. Song, X. Li, X. Wu, N. Brown, C. Naud, D. Mayou, T. Li, J. Hass, A.N. Marchenkov, E.H. Conrad, P.N. First, W.A. de Heer, “Electronic Confinement and Coherence in Patterned Epitaxial Graphene”, *Science*, 312(5777), 1191-1196, May 2006.

[28] K.S. Kim, Y. Zhao, H. Jang, S.Y. Lee, J.M. Kim, K.S. Kim, P. Kim, J.H. Ahn, J.Y. Choi, B.H. Hong, “Large-scale pattern growth of graphene films for stretchable transparent electrodes”, *Nature*, 457(7230),706-710, February 2009.

[29] X. Li, W. Cai, S. Kim, J. Nah, D. Yang, R. Piner, A Velamakanni, I. Jung, E. Tutuc, S.K. Banerjee, L. Colombo, R.S. Ruoff, “Large-Area Synthesis of High-Quality and Uniform Graphene Films on Copper Foils”, *Science*, 324(5932), 1312-1314, June 2009.

[30] S. Bhaviripudi, X. Jia, M.S. Dresselhaus, J. Kong, “Role of kinetic factors in chemical vapor deposition synthesis of uniform large area graphene using copper catalyst”, *Nano Letters,* 10(10), 4128-4133 October 2010.

[31] I. Vlassiouk, M. Regmi, P. Fulvio, S. Dai, P. Datskos, G. Eres, S. Smirnov, “Role of hydrogen in chemical vapor deposition growth of large single-crystal graphene”, *ACS Nano*, 5(7), 6069-6076, July 2011.

[32] Z. Yan, J. Lin, Z. Peng, Z. Sun, Y. Zhu, L. Li, C. Xiang, E. L. Samuel, C. Kittrell, J. M. Tour, "Toward the synthesis of water-scale single-crystal graphene on copper foils", *ACS Nano*, *6* (10), 9110–9117, October 2012.

[33] R. Van Noorden, "Production: Beyond sticky tape", *Nature*, 483(7389), S32-S33, March 2012.

[34] S. Bae, H. Kim, Y. Lee, X. Xu, J.-S. Park, Y. Zheng, J. Balakrishnan, T. Lei, H. R. Kim, Y. Il Song, Y.J. Kim, K. S. Kim, B. Özyilmaz, J.H. Ahn, B. H. Hong, S. Iijima, "Roll-to-roll production of 30-inch graphene films for transparent electrodes", *Nature Nanotechnology*, 5(8),574-578, August 2010.

[35] S.P. Koenig, "Graphene Membranes: Mechanics, Adhesion, and Gas Separations", Dissertation – University of Colorado, Boulder, 2013.

[36] Q.H. Wang, K. Kalantar-Zadeh, A. Kis, J.N. Coleman, M.S. Strano, "Electronics and optoelectronics of two-dimensional transition metal dichalcogenides", *Nature Nanotechnology*, 7,699–712, November 2012.

[37] G.R. Bhimanapati, Z. Lin, V. Meunier, Y. Jung, J. Cha, S. Das, et al. "Recent Advances in Two-Dimensional Materials beyond Graphene", *ACS Nano*, 9(12), 11509-11539, December 2015.

[38] D. Jena, "Tunneling Transistors Based on Graphene and 2-D Crystals", *Proceedings of the IEEE*, 101(7),1585-1599, July 2013.

[39] Y. P. Subbaiah, K. J. Saji, A. Tiwari, "Atomically Thin MoS_2: A Versatile Nongraphene 2D Material", *Advanced Functional Materials*, 26, 2046-2069, February 2016.

[40] K. He, C. Poole, K.F. Mak, J. Shan, "Experimental Demonstration of Continuous Electronic Structure Tuning via Strain in Atomically Thin MoS_2" *Nano Letters*, 13(6), 2931-2936, June 2013.

[41] D. Lloyd, X. Liu, J. W. Christopher, L. Cantley, A. Wadehra, B.L. Kim, B.B. Goldberg, J.S. Bunch, "Band Gap Engineering with Ultralarge Biaxial Strains in Suspended Monolayer MoS_2", *Nano Letters*, 16(9), 5836-5841 September 2016

[42] A. Splendiani, L. Sun, Y. Zhang, T. Li, J. Kim, C.Y. Chim, G. Galli, F. Wang, "Emerging photoluminescence in monolayer MoS_2", *Nano Letters*, 10(4), 1271-1275, March 2010.

[43] J.W. Jiang, "Graphene versus MoS_2: A Short Review", *Frontiers of Physics,* 10(3), 287-302, June 2015.

[44] S.Z. Butler, S.M. Hollen, L. Cao, Y. Cui, J.A. Gupta, H.R. Gutie, T.F. Heinz, S.S. Hong, J. Huang, A.F. Ismach, E. Johnston-Halperin, M. Kuno, V.V. Plashnitsa, R.D. Robinson, R.S. Ruoff, S. Salahuddin, J. Shan, L. Shi, M.G. Spencer, M. Terrones, W. Windl, J.E. Goldberger, "Progress, Challenges and Opportunities in Two-Dimensional Materials Beyond Graphene", *ACS Nano*, 7(4), 2898-2926, September 2013.

[45] K.F. Mak, C. Lee, J. Hone, J. Shan, T. F. Heinz, "Atomically thin MoS_2: A new direct-gap semiconductor", *Physical Review Letters*, 105:136805, September 2010.

[46] M. Chhowalla, H.S. Shin, G. Eda, L.J. Li, K.P. Loh, H. Zhang, "The Chemistry of two-dimensional layered transition metal dichalcogenide nanosheets", *Nature Chemistry,* 5(4), 263-275, April 2014.

[47] R.M. Yunus, H. Endo, M. Tsuji, H. Ago, "Vertical heterostructures of MoS2 and graphene nanoribbons grown by two-step chemical vapor deposition for high-gain photodetectors", *Physical Chemistry Chemical Physics*, 17(38), 25210-2515, September 2015.

[48] X. Cui, G. H. Lee, Y. D. Kim, G. Arefe, P. Y. Huang, C. Lee, D. A. Chenet, X. Zhang, L. Wang, F. Ye, F. Pizzocchero, B. S. Jessen, K. Watanabe, T. Taniguchi, D. A. Muller, T. Low, P. Kim and J. Hone, "Multi-terminal transport measurements of MoS_2 using a van der Waals heterostructure device platform", *Nature Nanotechnology*, 10(6), 534-540 June 2015.

[49] F. Ye, J. Lee, P.X. Feng, "Atomic layer MoS2-graphene van der Waals heterostructure nanomechanical resonators", *Nanoscale*, 9(46), 18208-18215, October 2017.

[50] Y.K. Koh, M.H. Bae, D.G. Cahill, E. Pop, "Reliably counting atomic planes of few-layer graphene (n > 4)", *ACS Nano*, 5(1), 269-274, January 2011.

[51] G. Cançado, A. Jorio, E.H.M. Ferreira, F. Stavale, C.A. Achete, R.B. Capaz, M.V.O. Moutinho, A. Lombardo, T.S. Kulmala, A.C. Ferrari, "Quantifying defects in graphene via Raman spectroscopy at different excitation energies." *Nano Letters*, 11(8), 3190-3106, August 2011.

[52] T.M.G. Mohiuddin, A. Lombardo, R.R. Nair, A. Bonetti, G. Savini, R. Jalil, N. Bonini, D.M. Basko, C. Galiotis, N. Marzari, K.S. Novoselov, A.K. Geim, A.C. Ferrari, "Uniaxial strain in graphene by Raman spectroscopy: G peak

splitting, Grüneisen parameters, and sample orientation", *Physical Review B*, 79(20):205433, May 2009.

[53] A. Balandin, S. Ghosh, W. Bao, I. Calizo, D. Teweldebrhan, F. Miao, C.N. Lau, "Superior thermal conductivity of single-layer graphene." *Nano Letters*, 8(3), 902-907, March 2008.

[54] A.C. Ferrari, D.M. Basko, "Raman spectroscopy as a versatile tool for studying the properties of graphene", *Nature Nanotechnology*, 8(4),235-246 April 2013.

[55] M. Ye, D. Winslow, D. Zhang, R. Pandey, Y.K. Yap, "Recent Advancement on the Optical Properties of Two-Dimensional Molybdenum Disulfide (MoS_2) Thin Films", *Photonics*, *2*(1), 288-307, January 2015.

[56] S. P. Timoshenko, S. W. Krieger, *Theory of Plates and Shells*, Second McGraw-Hill Book Company, 1959.

[57] K.L. Mittal, "Adhesion Measurement of Thin Films", *ElectroComponent Science and Technology*, 3(1),21-42, August 1975.

[58] B.N. Chapman, "Thin-film adhesion", *Journal of Vacuum Science and Technology*, 11, 106-113, January 1974.

[59] J. Valli, "A review of adhesion test methods for thin hard coatings." *Journal of Vacuum Science & Technology*, 4, 3007-3014, November 1986.

[60] A. Sofla, E. Seker, J.P. Landers, M.R. Begley, "PDMS-Glass Interface Adhesion Energy Determined Via Comprehensive Solutions for Thin Film Bulge/Blister Tests", *Journal of Applied Mechanics*, 77(3):031007, May 2010.

[61] J.E. Pawel, C.J. McHargue, "Testing of adhesion of thin films to substrates", *Journal of Adhesion Science and Technology*, 2(1), 396-383, January 1988.

[62] J.E.E. Banglin, "Interface design of thin film adhesion", In, L.-H. Lee (ed.) *Fundamentals of Adhesion*, 1991. New York: Plenum Press.

[63] J.G. Williams, "Energy release rates for the peeling of flexible membranes and the analysis of blister tests", *International Journal of Fracture*, 87(3), 265-288, October 1997.

[64] R. Jacobsson, B. Kruse, “Measurement of adhesion of thin evaporated films on glass substrates by means of the direct pull method”, *Thin Solid Films*, 15(1),71-77, January 1973.

[65] K. Kendall, “The adhesion and surface energy of elastic solids.” *Journal of Physics D: Applied Physics*, 4,1186-1195, August 1971.

[66] H. Mastrangelo, C. H. Hsu, “A simple experimental technique for the measurement of the work of adhesion of microstructures”, *Technical Digest IEEE Solid-State Sensor and Actuator Workshop*, 208-212, June 1992. DOI: 10.1109/SOLSEN.1992.228291

[67] J. Israelachvilli, *Intermolecular and Surface Forces*, Third Edition, 2011. Academic Press.

[68] J.G. Williams, “Energy Release Rates for the Peeling of Flexible Membranes and the Analysis of Blister Tests”, *International Journal of Fracture*, 87(3),265-288, October 1997.

[69] H. Hencky, “Uber den spannungzustand in kreisrunden platten mit verschwindender biegungssteiflgeit”, *Zeitschrift für Mathematik und Physik*, 63, 311–317,1915.

[70] W.B. Fichter, “Some Solutions for the Large Deflections of Uniformly Loaded Circular Membranes,” *NASA Technical Paper*, 3658, 1997.

[71] N.G. Boddeti, S.P. Koenig, L. Rong, J. Xiao, J.S. Bunch, M.L. Dunn, “Mechanics of Adhered Pressurized Graphene Blisters”, *Journal of Applied Mechanics*, 80:040909, May 2013.

[72] T.Higashi, S.J. Sweeney, A.F. Phillips, A.R. Adams, E. O’Reilly, T. Uchida, T. Fujii, “Experimental analysis of temperature dependence in 1.3mu/m AlGaInAs-InP strained MQW lasers”, *IEEE Journal of Selected Topics in Quantum Electronics*, 5(3),413-419, May 1999.

[73] A. Steinhoff, J.H. Kim, F. Jahnke, M. Rösner, D.S. Kim, C. Lee, G.H. Han, M.S. Jeong, T.O. Wehling, C. Gies, “Efficient Excitonic Photoluminescence in Direct and Indirect Band Gap Monolayer MoS_2”, *Nano Letters*, 15(10), 6841-6847, August 2015.

[74] Y.Y. Hui, X. Liu, W. Jie, N.Y. Chan, J. Hao, Y.T Hsu, L.J. Li, W. Guo, S.P. Lau, “Exceptional tenability of bang energy in a compressively strained trilayer MoS_2 sheet.”, *ACS Nano*, 7(8),7126-7131, 2013.

[75] S. Manzeli, A. Allain, A. Ghadimi, A. Kis, "Piezoresistivity and Strain-induced Band Gap Tuning Atomically Thin MoS_2", *Nano Letters*, 15(8), 5330-5335, July 2015.

[76] D. Pierucci, H. Henck, J. Avila, A. Balan, C.H. Naylor, G. Patriarche, Y.J. Dappe, M.G. Silly, F. Sirotti, A.T.C. Johnson, M.C. Asensio, A. Ouerghi, "Band Alignment and Minigaps in Monolayer MoS_2-Graphene van der Waals Heterostructures", *Nano Letters*, 16(7), 4054-4061, June 2016.

[77] S. Bhaviripudi, X. Jia, M. S. Dresselhaus, J. Kong, "Role of kinetic factors in chemical vapor deposition synthesis of uniform large area graphene using copper catalyst.", *Nano Letters*, 10(10), 4128-4133, September 2010.

[78] I. Vlassiouk, M. Regmi, P. Fulvio, S. Dai, P. Datskos, G. Eres, S. Smirnov, "Role of Hydrogen in Chemical Vapor Deposition Growth of Large Single-Crystal Graphene", *ACS Nano*, 5(7), 6069-6076, July 2011.

[79] C.Lee, H. Yan, L.E. Brus, T. F. Heinz, J. Hone, S. Ryu, "Anomalous Lattice Vibrations of Single-and Few-Layer MoS_2", *ACS Nano,* 4(5), 2695-2700, May 2010.

[80] Y.Y. Wang, Z.H. Ni, T. Yu, Z.X. Shen, H.M. Wang, Y.H Wu, W. Chen, A.T. Shen Wee, "Raman Studies of Monolayer Graphene: The Substrate Effect"*, Physical Chemistry C*, 112, 10637-10640, June 2008.

[81] X. Chen, L. Zhang, S. Chen, "Large area CVD growth of graphene", *Synthetic Metals 210*, 210(Part A), 95-108, December 2015.

[82] Y. Zhang, L. Zhang, C. Zhou, "Review of Chemical Vapor Deposition of Graphene and Related Applications", *Accounts of Chemical Research,* 46(10), 2329-2339, March 2013.

[83] V. Yokaribas, S. Wagner, D.S. Schenider, P. Friebertshauser, M.C. Lemme, C.P. Fritzen, "Strain Gauges Based on CVD Graphene Layers and Exfoliated Graphene Nanoplatelets with Enhanced Reproducibility and Scalability for Large Quantities", *Sensors*, 17(12), pii: E2937, December 2017.

[84] R.J.T. Nicholl, N.V. Lavrik, I. Vlassiouk, B.R. Srijanto, K.I. Bolotin, "Hidden Area and mechanical nonlinearities in freestanding graphene.", *Physical Review Letters*, 118(26), 266101, June 2017.

[85] J. D. Campbell, "On the theory of initially tensioned circular membranes subjected to uniform pressure," *The Quarterly Journal of Mechanics and Applied Mathematics*, 9(1), 84–93, January 1956.

[86] E. Khestanova, F. Guinea, L. Fumagalli, A.K. Geim, I.V. Grigorieva, "Universal shape and pressure inside bubbles appearing in van der Waals heterostructures", *Nature Communications*, 7:12587, August 2016.

[87] M.Y. Li, C.H. Chen, Y. Shi, L.J. Li, "Heterostructures based on two-dimensional layered materials and their potential applications", *Materials Today*, 19(6), 322-335, August 2016.

[88] R. C. Cooper, C. Lee, C. A. Marianetti, X. Wei, J. Hone, J. W. Kysar, "Nonlinear elastic behavior of two-dimensional molybdenum disulfide", *Physical Review B*, 87, 035423, January 2013.

[89] H. Zhu, Y. Wang, J. Xiao, M. Liu, S. Xiong, Z. J. Wong, Z. Ye, Y. Ye, X. Yin, X. Zhang, "Observation of piezoelectricity in free-standing monolayer MoS_2", *Nature Nanotechnology*, 10(2), 151-155, February 2015.

[90] A. Castellanos-Gomez, R. Roldan, E. Cappelluti, M. Buscema, F. Guinea, H. S. J. Van Der Zant, G. A. Steele, "Local strain engineering in atomically thin MoS_2", *Nano Letters*, 13(11), 5361-5366, October 2013.

[91] A. D. Smith, F. Niklaus, A. Paussa, S. Schröder, A. C. Fischer, M. Sterner, S. Wagner, S. Vaziri, F. Forsberg, D. Esseni, M. Östling, M. C. Lemme, "Piezoresistive Properties of Suspended Graphene Membranes under Uniaxial and Biaxial in Nanoelectromechanical Pressure Sensors", *ACS Nano,* 10(11), 9879-9886, November 2016.

[92] S. Bertolazzi, J. Brivio, A. Kis, "Stretching and Breaking of Ultrathin MoS_2", *ACS Nano*, 5(12), 9703-9709, November 2011.

[93] Z. Shi, H. Lu, L. Zhang, R. Yang, Y. Wang, D. Liu, H. Guo, D. Shi, H. Gao, E. Wang, G. Zhang, "Studies of Graphene-Based Nanoelectromechanical Switches", *Nano Research*, 5(2), 82–87, December 2011.

[94] C.J. Shearer, A.D. Slattery, A.J. Stapleton, J.G. Shapter, C.T. Gibson, "Accurate thickness measurement of graphene", *Nanotechnology*, 27(12):125704, March 2016.

[95] C. Androulidakis, E.N. Koukaras, J. Parthenios, G. Kalosakas, K. Papagelis, C. Galiotis, "Graphene flakes under controlled biaxial deformation", *Scientific Reports*, 5:18219, December 2015.

[96] Y. Kobayashi, T. Taniguchi, K. Watanabe, Y. Maniwa, Y. Miyata, "Slidable atomic layers in var der Walls heterostructures", *Applied Physics Express*, 10(4): 045201, March 2017.

[97] Hedberg,J.(n.d.),(http://www.jameshedberg.com/scienceGraphics.php?sort=all&id=graphene-atomic-structure-sheet).

[98] D. Akinwande, C. J. Brennan, J. Scott Bunch, P. Egberts, J. R. Felts, H. Gao, R. Huang, J. Kim, T. Li, Y. Li, K. M. Liechti, N. Lu, H. S. Park, E. J. Reed, P. Wang, B. I. Yakobson, T. Zhang, Y. Zhang, Y. Zhou, Y. Zhu, "A Review on Mechanics and Mechanical Properties of 2D Materials – Graphene and Beyond", *Extreme Mechanics Letters*, 13, 42-77, May 2017.

[99] B.J. Briscoe, S.S. Panesar, "The application of the blister test to an elastomeric adhesive." *Proceedings of the Royal Society. A, Mathematical, Physical and Engineering Sciences*, 433(1887), 23-43, April 1991.

[100] J.E.E. Banglin, "Interface design of thin film adhesion", In, L.-H. Lee (ed.) *Fundamentals of Adhesion*, 1991. New York: Plenum Press.

[101] K. Wan, Y. Mai, "Modified blister tests for evaluation of thin flexible membrane adhesion on rigid substrate", *Materials Science Research International*, *1*(2), 78-81, March 1995.

[102] K. Wan, Y. Mai, "Fracture mechanics of a new blister test with stable crack growth", *Acta Metallurgica et Materialia*, 43(11), 4109-4115, November 1995.

[103] H. Dannenberg, "Measurement of adhesion by a blister method", *Applied Polymer Science*, 5(14), April 1961.

[104] R. Escobar Galindo, A. van Veen, J.H. Evans et al., "A modified blister test to the adhesion of thin coating based on local helium ion implantation", *Thin Solid Films*, 471(1-2), 170-176, January 2005.

[105] B. Radisavljevic, A. Radenovic, J. Brivio, V. Giacometti, A, Kis, "Single-layer MoS_2 Transistors", *Nature Nanotechnology*, 6(3), 147-150, March 2011.

[106] D.Lloyd, X. Liu, N. Boddeti, L. Cantley, R. Long, M. L. Dunn, J. S. Bunch, "Adhesion, stiffness, and Instability in Atomically Thin MoS_2 bubbles", *Nano Letters*, 17(9), 5329-5334, September 2017.

CURRICULUM VITAE

[redacted]